ARTICLE

Dbnl and β-catenin promote pro-N-cadherin processing to maintain apico-basal polarity

Antonio Herrera, Anghara Menendez, Blanca Torroba, Andrea Ochoa, and Sebastián Pons

The neural tube forms when neural stem cells arrange into a pseudostratified, single-cell–layered epithelium, with a marked apico-basal polarity, and in which adherens junctions (AJs) concentrate in the subapical domain. We previously reported that sustained β-catenin expression promotes the formation of enlarged apical complexes (ACs), enhancing apico-basal polarity, although the mechanism through which this occurs remained unclear. Here, we show that β-catenin interacts with phosphorylated pro-N-cadherin early in its transit through the Golgi apparatus, promoting propeptide excision and the final maturation of N-cadherin. We describe a new β-catenin–dependent interaction of N-cadherin with Drebrin-like (Dbnl), an actin-binding protein that is involved in anterograde Golgi trafficking of proteins. Notably, Dbnl knockdown led to pro-N-cadherin accumulation and limited AJ formation. In brief, we demonstrate that Dbnl and β-catenin assist in the maturation of pro-N-cadherin, which is critical for AJ formation and for the recruitment AC components like aPKC and, consequently, for the maintenance of apico-basal polarity.

Introduction

In the embryonic neural tube (NT), neural stem cells (NSCs) form a pseudostratified, single-cell–layered epithelium that extends from the ventricle to the basal lamina and that displays marked apico-basal polarity. The proteins present in the apical pole of NSCs are collectively called the apical complex (AC), and they were initially described in the cerebral cortex. The AC establishes three concentric subdomains with discrete functions: The fate-determining factors (PAR3, aPKC, and Prominin-1) remain confined within or close to the apical membrane; the zonular proteins (ZO1, Afadin, and actin) occupy an intermediate position; and the junctional complexes (N-cadherin, α-catenin, and β-catenin) are located in the subapical domain (Marthiens and ffrench-Constant, 2009). However, although different AC proteins are enriched in these domains, there is extensive overlap in their distributions.

During development, NSCs can initially be identified by the expression of Sox2 or CD133/Prominin-1 (Zhu et al., 2009), and these cells proliferate symmetrically in a self-expanding mode. Later on and in association with the onset of neurogenesis, their mode of division changes to generate the first committed neurons (Götz and Huttner, 2005; Saade et al., 2013). In these neurogenic divisions, postmitotic NSCs diminish their N-cadherin expression, and they detach from the proliferative ventricle (Das and Storey, 2014; Rousso et al., 2012). Thus, it is critical to coordinate NSC differentiation and delamination in order to establish the correct architecture of the nervous system.

β-catenin mediates canonical Wnt signaling, stimulating Tcf-dependent transcription (Grigoryan et al., 2008; Nelson and Nusse, 2004). However, β-catenin also plays important roles in epithelial cell polarity, for example, associating with classic cadherins through its armadillo domains and thereby contributing to the formation of adherens junctions (AJs; Baum and Georgiou, 2011). Classic cadherins share a basic structure and role in adherence, and they are named on the basis of the tissue in which they are mainly expressed (i.e., E-cadherin in epithelial tissue, N-cadherin in neural tissue). These glycoproteins are synthesized as precursors that must undergo a series of post-translational modifications to become functional at AJs. The association between the mature form of classic cadherins and β-catenin has been widely studied; however, the relationship between β-catenin and the precursor pro-cadherins is still poorly understood.

We previously reported that sustained expression of β-catenin in the developing NT promoted the formation of enlarged ACs, and although these cells remained as progenitors, this modification increased polarization and adhesiveness, limited proliferation (Herrera et al., 2014), and reduced

delamination and migration (Rabadán et al., 2016). Here, we studied the molecular mechanisms by which β-catenin promotes AC formation in NSCs. We show that β-catenin binds to phosphorylated pro-N-cadherin early in the secretory pathway, specifically in the ER/cis-Golgi compartment, promoting the excision of the propeptide and its final maturation into N-cadherin. In this regard, we describe a new β-catenin–dependent interaction of N-cadherin with Dbnl, an actin-binding protein active in anterograde protein trafficking through the Golgi apparatus. Notably, we show that Dbnl knockdown impedes N-cadherin maturation, causing pro-N-cadherin accumulation in NSCs. We also demonstrate that β-catenin–driven maturation of N-cadherin requires Dbnl and that it is indispensable for the formation of AJs and the recruitment of other AC components (e.g., aPKC) and, accordingly, for the establishment and maintenance of apicobasal polarity. The effect of β-catenin on N-cadherin maturation is independent of transcription, and remarkably, we demonstrate that the persistence of pro-N-cadherin leads to the loss of the apical AJs in proliferating NSCs. As a result, these cells either invade the ventricle or prematurely delaminate due to the retraction of the apical process. Therefore, we conclude that β-catenin–assisted maturation of N-cadherin is required not only to maintain apico-basal polarity but also to preserve NT integrity.

Results

β-catenin promotes the association of aPKCι with N-cadherin

In the neuroepithelium of the telencephalon, aPKC is located more apically than N-cadherin/β-catenin within the AC (Marthiens and ffrench-Constant, 2009). Similarly, in the Hamburger and Hamilton stage 16 (HH16) chicken spinal cord neuroepithelium (Fig. 1 A), most of the aPKC was detected apical to N-cadherin/β-catenin, although a significant amount of aPKC colocalized with N-cadherin/β-catenin at the boundary between the apical and subapical regions (Fig. 1, B and C). Coimmunoprecipitation has been widely used to detect protein–protein interactions, but this technique requires efficient antibodies and strong protein–protein interactions, such as those recently described for heterodimers of E-cadherin and N-cadherin (Rogers et al., 2018). However, we found that mild and/or transitory interactions not detected by normal coimmunoprecipitation were evident when a combination of mild crosslinking and the Strep-tag/Strep-Tactin purification system was used. This system allows ionic detergents to be used to solubilize the sample and for the column binding and high stringency washes. In addition, elution is performed by competitive affinity binding at isotropic conditions, displaying high sensitivity and specificity, even for very weak interactions (Klockenbusch and Kast, 2010; Kubben et al., 2010).

To examine the interactions between N-cadherin, aPKCι, and β-catenin, we electroporated HH12 chicken embryos with Strep-tag (ST)-tagged forms of these three molecules individually (Fig. 1 D), and we then purified these proteins 24 h post-electroporation (hpe; corresponding to stage HH18) on Strep-Tactin affinity columns (Fig. 1 E). The endogenous partners of these proteins were examined in Western blots (Fig. 1, F–H), demonstrating that β-catenin-ST and aPKCι-ST efficiently

copurified the other two partners (Fig. 1, F and G). By contrast, N-cadherin-ST copurified β-catenin but almost no aPKCι (Fig. 1 H). Interestingly, β-catenin transfection significantly increased the amount of endogenous aPKCι that copurified with N-cadherin-ST (Fig. 1 I), indicating that N-cadherin binding to aPKC was mediated by β-catenin. Indeed, N-cadherinΔβcat-ST, a mutant N-cadherin lacking the β-catenin–binding domain, did not copurify with either β-catenin or aPKCι (Fig. 1 J).

β-catenin induces the apical localization of aPKC through its binding to N-cadherin

We previously demonstrated that stable forms of β-catenin induced aberrant growth of the neuroepithelium by enhancing the accumulation of AC proteins at the apical pole of NSCs (Herrera et al., 2014). This phenotype required aPKCι, and it could not be entirely reproduced by constitutive activation of the Wnt pathway through Tcf3·Vp16. As a result, we hypothesized that the structural and transcriptional activities of β-catenin were required to deliver N-cadherin and aPKC to the AC. As mentioned above, β-catenin binds N-cadherin in the AC, linking the AJs to the actin cytoskeleton, but it also binds to Tcf transcription factors, displacing Groucho, a transcriptional repressor. We refer to these two activities of β-catenin as structural and transcriptional because they regulate cell structure and gene transcription, respectively. Notably, the interaction of β-catenin with N-cadherin and Tcf is mediated in both cases by the armadillo domains of β-catenin, such that changes in β-catenin expression will necessarily affect both activities. By contrast, Tcf3·Vp16 is a constitutive transcription activator that interacts directly with TCF binding motifs on DNA but not with β-catenin (Herrera et al., 2014), and thus, it would induce only β-catenin–like transcription activation. In addition, N-cadherinΔβcat is a truncated form of N-cadherin that does not bind β-catenin, preventing β-catenin binding to the AC and inhibiting its structural activity without affecting its capacity to interact with Tcf.

To decipher the contribution of each of these activities to the formation/maintenance of the AC and consequently, to the integrity of the neural epithelium, we studied the distribution of N-cadherin and aPKC under different conditions where the structural and transcriptional activities of β-catenin were modified independently (see Fig. 2 and Fig. S1 for complete images). The apico-basal distribution of aPKC and N-cadherin expression at 48 hpe was studied in images normalized to 100 pixels (the first 15 were considered apical and the remaining 85 basolateral; Fig. 2, A–F), and the pixel intensity profiles for aPKC and N-cadherin were plotted, normalizing the maximum value to 1, and then the area under the curve calculated for the apical ($\int_A$) and basolateral ($\int_{BL}$) regions (Fig. 2, G–L). Finally, and as an indicator of neuroepithelial polarization, we calculated the apico/basolateral (A/BL) ratios of aPKC and N-cadherin, normalized to their respective controls, to facilitate a comparison between these two proteins: $(\int_A/\int_{BL})^{Control}/(\int_A/\int_{BL})^{Treatment}$ (Fig. 2, G′–L′). In addition, we calculated the incidence of invagination and lumen invasion associated with the different treatments (Fig. 2, M–R). The expression of β-catenin ("structural and transcriptional up") induced the formation of larger ACs that contained more aPKC and N-cadherin (Fig. 2, B, H, and
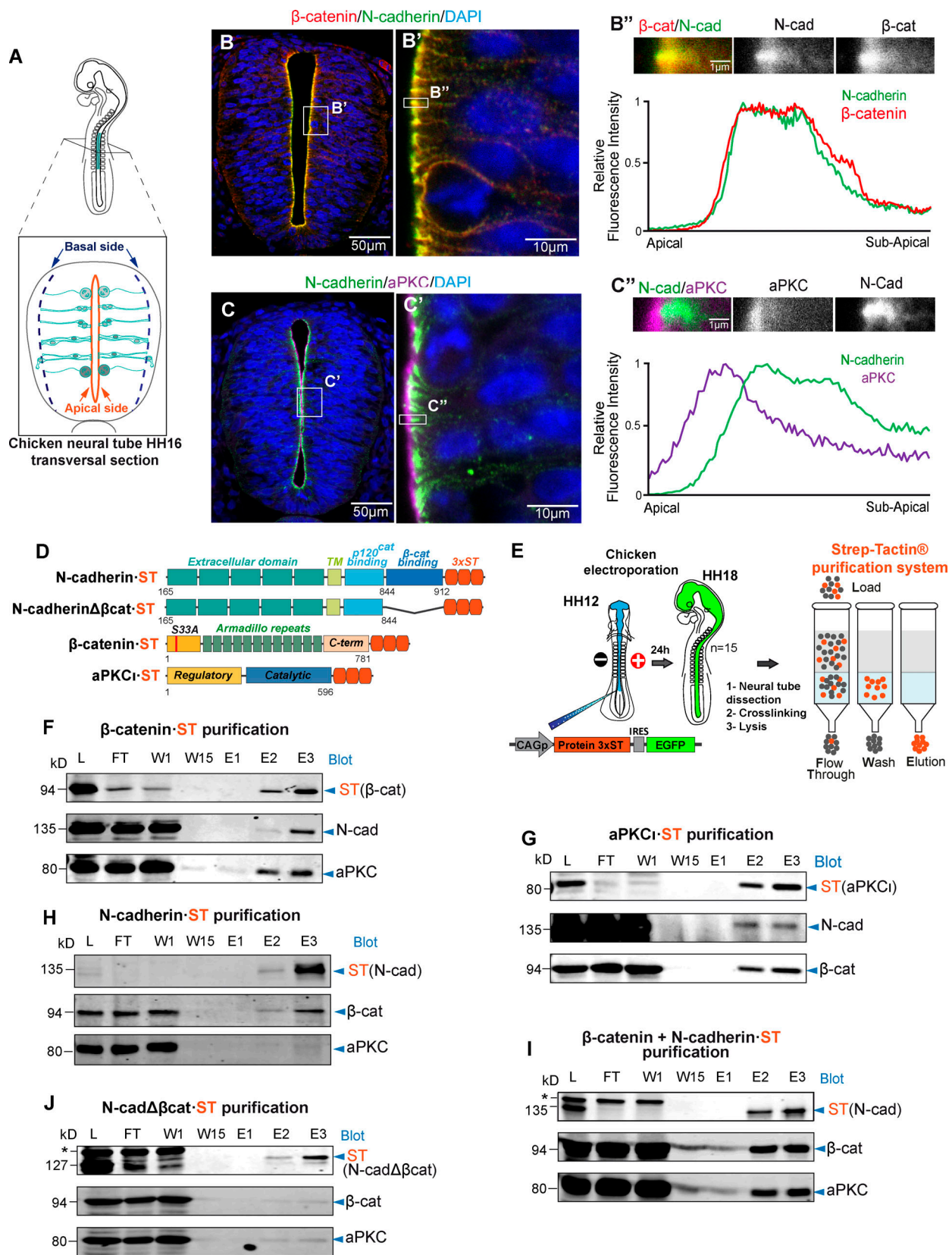
Herrera et al.
Dbnl and β-catenin promote N-cadherin maturation

Journal of Cell Biology 2 of 19
https://doi.org/10.1083/jcb.202007055

Figure 1. β-catenin promotes the association of aPKCι with N-cadherin. (A) Representation of HH16 chicken NT slices. **(B)** Slices were stained with antibodies against β-catenin (red), N-cadherin (green), and DAPI (blue); the area labeled as B' is enlarged in the right-hand panel. The graph shows the relative pixel intensity profile for N-cadherin and β-catenin in the area labeled as B'', with the area quantified shown above. The two channels are displayed separately in grayscale for clarity. **(C)** As in B but using antibodies against N-cadherin and aPKCι. **(D)** Scheme of the four ST-tagged molecules used. **(E)** Representation of

the in ovo electroporation and Strep-tag/Strep-Tactin purification procedures; 15 embryos (HH18 embryos) were used for each purification. **(F–J)** The different ST-tagged proteins were electroporated for 24 h into HH12 chicken NTs, and the ST-tagged and associated endogenous proteins were purified on Strep-Tactin columns at HH18. **(F)** Electroporation and purification of β-catenin·ST probed with antibodies against ST (β-catenin), N-cadherin, and PKCι. **(G)** Electroporation and purification of aPKCι·ST probed with antibodies against ST (aPKCι), N-cadherin, and β-catenin. **(H)** Electroporation and purification of N-cadherin·ST probed with antibodies against ST (N-cadherin), β-catenin, and aPKCι. **(I)** Electroporation of N-cadherin·ST plus untagged β-catenin. Purified proteins were probed with antibodies against ST (N-cadherin), β-catenin, and aPKCι. Note that electroporation of β-catenin substantially increased the amount of aPKC that copurified with N-cadherin·ST. **(J)** Electroporation and purification of N-cadherinΔβcat·ST probed with antibodies against ST (N-cadherinΔβcat), β-catenin, and PKCι. Note that neither β-catenin nor PKCι copurify with N-cadherinΔβcat·ST. In I and J, the asterisk indicates a nonspecific band. cad, cadherin; C-term, C-terminus; E, elution; FT, flow through; L, lysate; W, wash.

N), causing a characteristic tissue invagination (Herrera et al., 2014). By contrast, β-catenin silencing with Sh-CTNNB1 ("structural and transcriptional down") reduced the amount of N-cadherin at the apical membrane, favoring a round shape of NSCs and inducing ventricle invasion by groups of transfected cells (Fig. 2, C, I, and O). Hence, a deficit in β-catenin impairs AJ function, compromising the cohesion of the epithelium in a manner consistent with the phenotype reported for the β-catenin knockout (Valenta et al., 2011).

Transfection of Tcf3·Vp16 (transcriptional up) induced aPKC and N-cadherin accumulation in the AC, provoking small invaginations similar to those produced by β-catenin transfection. However, although Tcf3·Vp16 stimulated the expression of aPKC similarly to β-catenin, the A/BL ratio of aPKC was reduced because it mostly remained in the basolateral compartment (Fig. 2, D, J, and P). Interestingly, coexpression of Tcf3·Vp16 with Sh-CTNNB1 (structural down and transcriptional up) disrupted the epithelium and the formation of NSC ACs, generating an unpolarized cell mass in the lumen. This response highlights the importance of β-catenin's structural activity for aPKC accumulation in the AC (Fig. 2, E, K, and Q). Notably, a very similar phenotype was obtained with a mutant N-cadherin that lacks the β-catenin–binding domain (N-cadherinΔβcat; Fig. 2, F, L, and R). In brief, β-catenin transcriptional activity induces the expression of proteins that like aPKC are relevant for AC formation and cell polarization. However, the structural function of β-catenin is an absolute requirement to construct ACs, to maintain apico-basal polarity, and to ensure the integrity of the neuroepithelium. Moreover, the structural activity of β-catenin involves its binding to N-cadherin.

β-catenin associates with N-cadherin in the Golgi apparatus

To reveal the cellular compartments in which N-cadherin interacts with aPKC and β-catenin, we calculated the Manders correlation coefficients for aPKC/N-cadherin and β-catenin/N-cadherin. The coefficient for aPKC/N-cadherin was significantly higher in the AC (0.41 ± 0.04) than in the rest of the cell (basolateral), where it was close to 0 (0.03 ± 0.01). Hence, aPKC appears to colocalize with N-cadherin almost exclusively in the AC (Fig. 3, A and B). By contrast, while the β-catenin/N-cadherin coefficient was significantly higher in the AC (0.90 ± 0.02) than in the whole cell (0.63 ± 0.02), colocalization in this case was also evident in the region adjacent to the AC (Fig. 3 C). In this space, the staining of N-cadherin and β-catenin was punctate, and the degree of colocalization seemed to increase in the proximity of the AC. In the developing brain cortex, radial glia

have a very elongated Golgi apparatus located apical to the nucleus, and vesicular trafficking takes place perpendicular to the apico-basal axis (Taverna et al., 2016). We observed a similar Golgi distribution in the NSCs of the developing trunk NT (Fig. 3 D). Therefore, we calculated the colocalization index of N-cadherin/β-catenin in the Golgi, in the AC-to-Golgi, and in the AC regions (Fig. 3, E and F). Notably, the colocalization index increased steadily from the Golgi to the AC from 0.24 (± 0.03) in the Golgi region to 0.46 (± 0.03) in the AC-to-Golgi region to 0.90 (± 0.02) in the AC region (Fig. 3, E and F). β-catenin and N-cadherin colocalization was already detected in the Golgi apparatus, and it apparently increased in the proximity of the AC. However, this difference could have been overestimated by the fact that the N-cadherin antibody had a greater affinity for mature N-cadherin than for immature forms. By contrast, aPKC seemed to interact with the N-cadherin/β-catenin complex exclusively in the AC.

β-catenin drives the apical localization of N-cadherin

In the HH16 chicken NT, N-cadherin accumulates at the apical AJs of NSCs, whereas actin accumulates at both the apical and the basal poles (Fig. 3, G and H). While the β-catenin–binding domain of N-cadherin was required for N-cadherin to accumulate in the ACs (Fig. 2, F and L; and Fig. S1 L), it was not clear whether β-catenin promoted the stability/recycling of the preexisting N-cadherin or whether it facilitated the transport/maturation of the newly synthetized protein. We observed that an important proportion of the transfected N-cadherin-GFP fusion protein remained in the basolateral compartment (Fig. 3, I and K), which we believe reflected an imbalance between the endogenous β-catenin and the exogenous N-cadherin-GFP. Indeed, β-catenin transfection induced the translocation of N-cadherin-GFP from the basolateral compartment to the AC (Fig. 3, J and K). This "apicalizing" effect of β-catenin was also evident for actin (Fig. 3, J–L) possibly because β-catenin induced an enlargement of the ACs that consequently recruited more apical actin filaments (Herrera et al., 2014). These results suggested a role for β-catenin in the transport and/or maturation of N-cadherin.

β-catenin deficiency induces pro-N-cadherin accumulation in the trans-Golgi network (TGN)

We further assessed the effect of β-catenin on the transport and/or maturation of N-cadherin in HEK-293 cells, an epithelial kidney cell line that does not express endogenous N-cadherin. In these cells, most of the transfected chicken N-cadherin·ST accumulated close to the nucleus in what were presumably
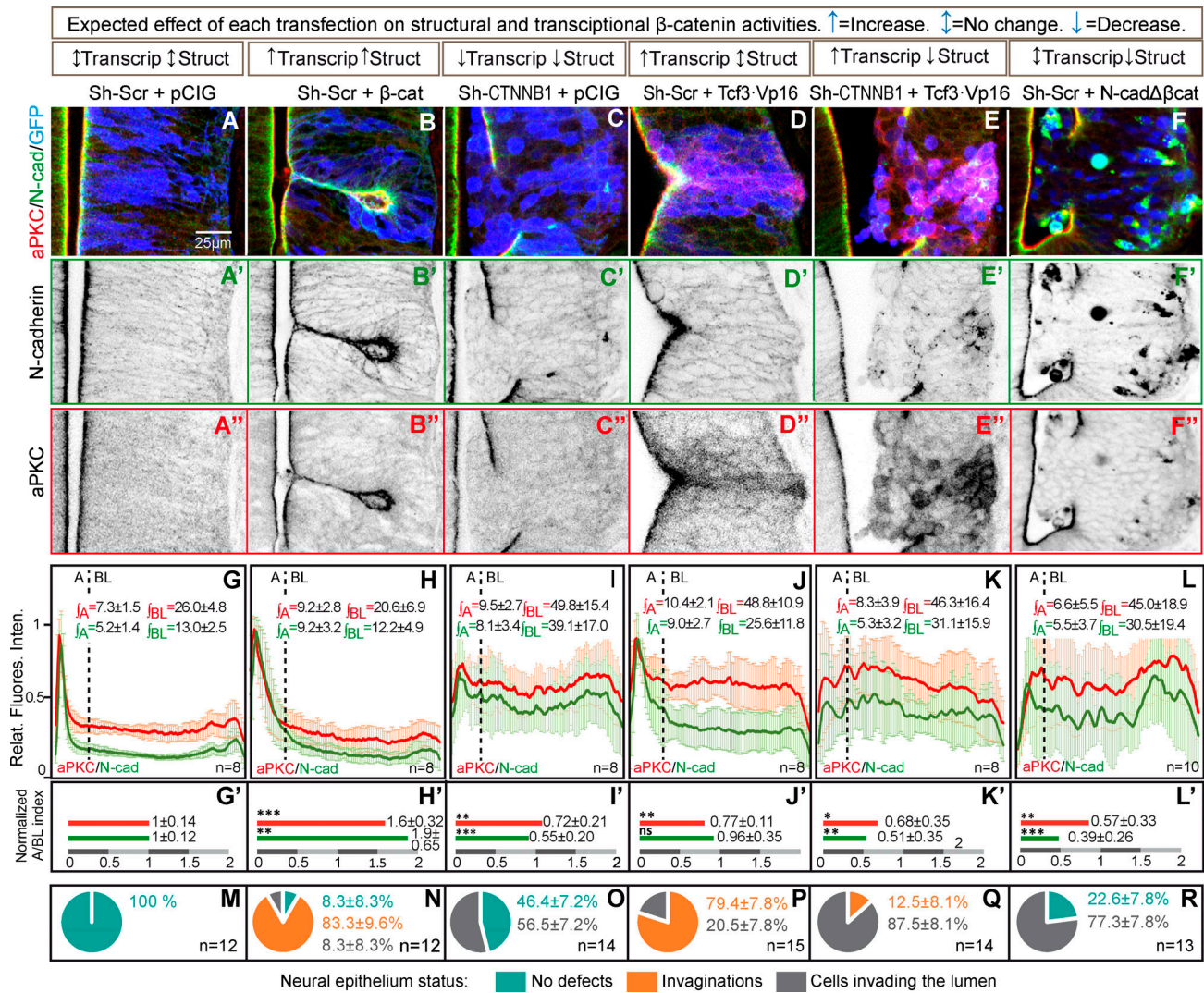
Figure 2. **β-catenin induces the apical localization of aPKC through its binding to N-cadherin. (A–F)** HH12 chicken NTs were transfected for 48 h with different molecular tools intended to independently manipulate the transcriptional (Transcrip) and structural (Struct) activities of β-catenin. The figure shows representative images at HH23 of the transfected NTs used for quantification and stained with N-cadherin (green), aPKC (red), and GFP (blue, indicates transfection). N-cadherin (A'–F') and aPKC (A''–F'') channels are shown separately in a grayscale below each red-green-blue image. The expected effect on transcriptional and structural activities is indicated in the boxes above each transfection combination. pCIG indicates the empty vector, and Sh-Scr and Sh-CTNNB1 the scrambled and the β-catenin inhibitory shRNAs, respectively. Tcf3·Vp16 is a constitutive activator of Tcf-dependent transcription, and N-cadherinΔβcat is an N-cadherin mutant lacking the β-catenin–binding domain. **(G–L)** The apico-basal distance in the images with a similar level of transfection was normalized to 100 pixels, with the first 15 pixels arbitrarily considered to be apical and the remaining 85 pixels basolateral. The line plots represent the relative pixel intensity profiles for aPKC and N-cadherin, and $\int_A$ and $\int_{BL}$ represent the values of the area under the curve for the apical and basolateral regions, respectively. The number of slices measured in each case (n) is displayed in the lower right corner. **(G'–L')** The bar charts represent the A/BL ratios of aPKC and N-cadherin expression normalized to their respective controls $[(\int_A/\int_{BL})^{Control}/(\int_A/\int_{BL})^{Treatment}]$; each experimental condition was compared with its control condition using an unpaired t test. **(M–R)** The pie charts represent the percentage of growth aberrations observed in each condition. The data are expressed as the mean ± SD; the number of slices measured in each case (n) is displayed in the lower right corner. *, $P < 0.05$; **, $P < 0.01$; ***, $P < 0.001$. cad, cadherin.

secretory vesicles (Fig. S2 A). Notably, transfected N-cadherin·ST relocated to the intercellular junctions when β-catenin was expressed in these cells (Fig. S2 B), whereas β-catenin failed to redistribute the mutant N-cadherin lacking the β-catenin–binding domain (Fig. S2, C and D). Indeed, subcellular fractionation of HEK-293 cells demonstrated that β-catenin enhanced the proportion of N-cadherin in the plasma membrane fraction relative to the internal membranes (Fig. S2 E). By contrast, N-cadherinΔβcat·ST was mainly found in the internal

membrane fraction, and it did not relocate to the plasma membrane following β-catenin expression (Fig. S2 E). To identify the step at which N-cadherin trafficking was blocked, we transfected HEK-293 cells with N-cadherin·ST (Fig. 4, A–F) or N-cadherinΔβCat·ST (Fig. 4, G–L) with (Fig. 4, B, D, F, H, J, and L) or without β-catenin (Fig. 4, A, C, E, G, I, and K), and we double stained the cells for ST and calreticulin (ER), GM130 (cis-Golgi), or Golgin97 (TGN). Neither N-cadherin·ST nor N-cadherinΔβcat·ST colocalized with calreticulin in either the
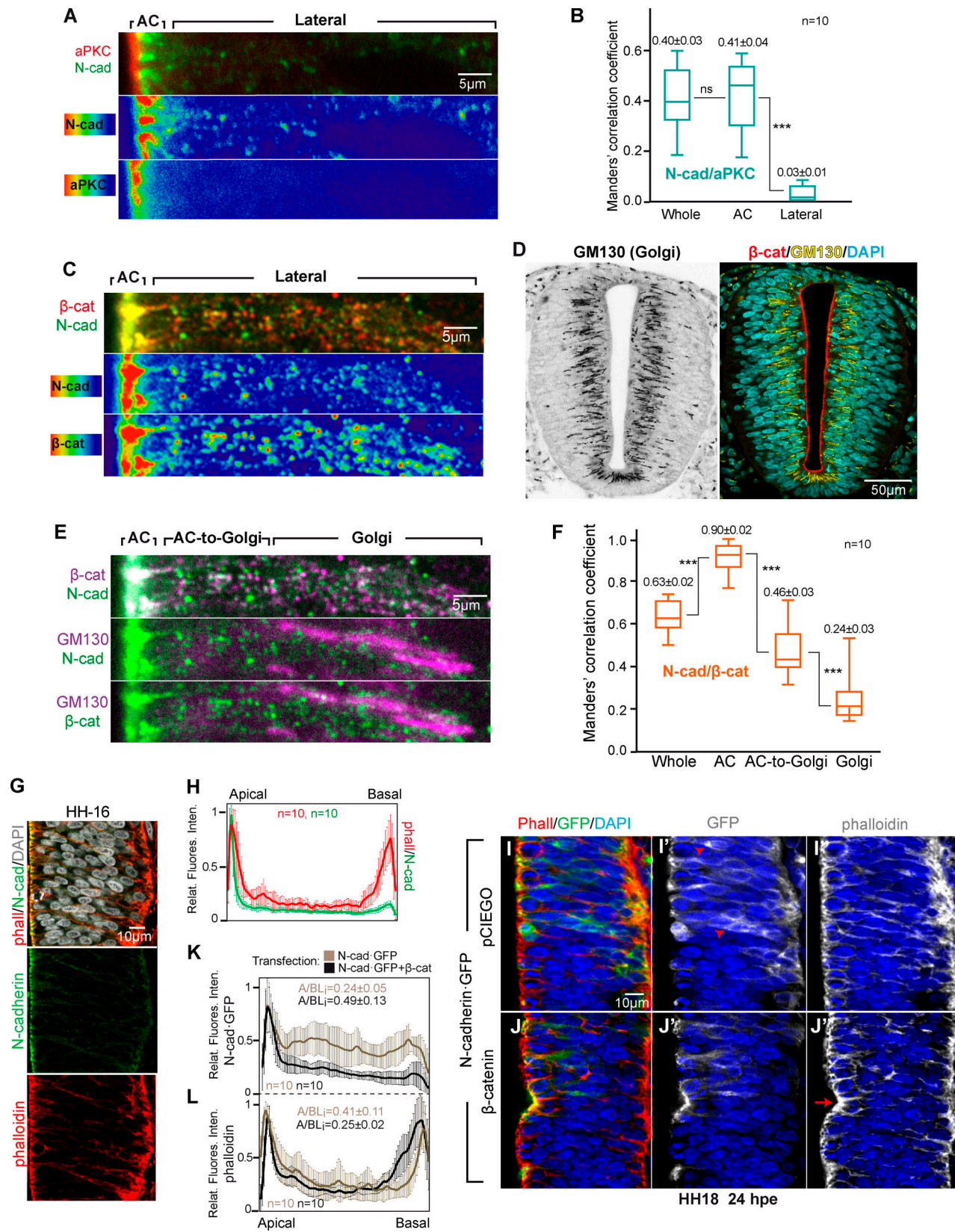
Figure 3. **β-catenin is associated to N-cadherin in the Golgi apparatus, and it promotes the accumulation of GFP-N-cadherin in the AC. (A)** High-magnification image of the apico-lateral region of HH16 NTs stained with aPKCι (red) and N-cadherin (green); the two lower panels show the N-cadherin and aPKCι channels separately using a high–low false color index. **(B)** Box plot showing the Manders correlation coefficients for N-cadherin and aPKCι (n = 10). **(C)** High–magnification image of the apico-lateral region of HH16 NTs stained for β-catenin (red) and N-cadherin (green). The two lower panels show the N-cadherin and β-catenin channels separately using a high-low false color index. **(D)** Grayscale and three-channel image of the Golgi apparatus (stained with

GM130) in the HH16 NT; β-catenin and DAPI are used as landmarks. **(E)** Same slice as in C, including GM130 staining; the three channels are shown two by two to reveal colocalization. The lateral region was divided into AC-to-Golgi and Golgi regions. **(F)** Box plot showing the Manders correlation coefficients for N-cadherin and β-catenin calculated for the areas described in panel E (n = 10). **(G and H)** Representative images and relative pixel intensity profiles of untransfected HH16 chicken NT slices stained with phalloidin to detect F-actin (red), anti-N-cadherin (green), and DAPI (gray); n = 10. **(I and J)** Representative images of HH18 chicken NTs at 24 hpe with N-cadherin·GFP, without (I–I'') or with (J–J'') β-catenin. Images show GFP (green, transfected N-cadherin-GFP) and phalloidin (red, F-actin). **(K)** Relative pixel intensity profiles of N-cadherin·GFP comparing images from I and J (n = 10). **(L)** Phalloidin profiles from the same images as in K (n = 10). For B and F, each experimental condition was compared with every other experimental condition using a one-way ANOVA with Tukey's multiple comparisons test. ***, P < 0.001. cad, cadherin; phall, phalloidin.

presence or the absence of β-catenin (Manders coefficient not shown). Although both N-cadherin·ST and N-cadherinΔβcat·ST colocalized with GM130, this colocalization was weak in both cases (Manders coefficients ranging from 0.21 ± 0.02 to 0.27 ± 0.05), and no significant differences were observed between the control and β-catenin–transfected cells (Fig. 4 M). By contrast, both N-cadherin·ST and N-cadherinΔβcat·ST colocalized strongly with Golgin97 (Manders 0.69 ± 0.06 and 0.73 ± 0.08). Interestingly, the colocalization of N-cadherin·ST and Golgin97 was significantly dampened after β-catenin transfection (Manders 0.69 ± 0.06 to 0.33 ± 0.07), while this did not affect the colocalization of N-cadherinΔβcat·ST with Golgin97 (Manders 0.69 ± 0.06 for control and 0.76 ± 0.04 for β-catenin; Fig. 4 M). It is worth noting that N-cadherin accumulation in the TGN was accompanied by an increase in the expression of Golgin97, consistent with protein accumulation in the TGN (Fig. 4, E, K, and L). In brief, a lack of β-catenin caused N-cadherin to accumulate in trans-Golgi vesicles, a situation that was reverted by the expression of β-catenin, which facilitated the delivery of N-cadherin to intercellular junctions.

N-cadherin is synthetized as a precursor that contains a propeptide at the N-terminus and that is excised during its maturation. To study the maturation of the N-cadherin accumulated in the TGN, we developed an antibody targeting the propeptide region (anti-pro-N-cadherin; Fig. 4 N). Using this antibody together with the anti-N-cadherin antibody that mainly recognized the mature form of N-cadherin (see Fig. 5 A for the characterization of these two antibodies), we observed that most of the accumulated N-cadherin·ST was pro-N-cadherin (Fig. 4 O) that was mainly observed in Golgin97-containing vesicles (Fig. 4 P).

β-catenin drives pro-N-cadherin conversion into mature N-cadherin by promoting propeptide cleavage

In untransfected HH16 chicken NT lysates, we detected two bands with the anti-pro-N-cadherin antibody developed in our laboratory and one with the commercial rat monoclonal antibody used here to detect N-cadherin (Fig. 5 A). The bands detected by the pro-N-cadherin and N-cadherin antibodies did not overlap, indicating that the N-cadherin antibody recognized mainly the mature form of N-cadherin. Similarly, N-cadherin·ST also separated into a similar three-band pattern (Fig. 5 B). Thus, we used HH18 (HH12 + 24 hpe) chicken NTs to study the consequences of β-catenin knockdown or overexpression on N-cadherin processing. We calculated the N-cadherin/pro-N-cadherin ratio for each transfection and normalized them to the control transfected lanes in which the ratio was considered as 1. Notably, β-catenin knockdown severely reduced the conversion of the upper band of pro-N-cadherin into mature N-cadherin (N-cadherin/pro-N-

cadherin[upper band] ratio = 0.49 ± 0.24), whereas β-catenin expression strongly enhanced its maturation (N-cadherin/pro-N-cadherin[upper band] ratio = 6.08 ± 0.63; Fig. 5 B). Pro-N-cadherin contains a furin cleavage site (Nakayama, 1997) that would be acted on in the TGN or in the space between this compartment and the cell surface to generate mature N-cadherin. Interestingly, furin only acted weakly on an N-cadherin mutant lacking the β-catenin–binding domain (Fig. S3, A and B). These results indicated that β-catenin directly promoted pro-N-cadherin propeptide cleavage, yet to understand the mechanisms involved, we had to first decipher the molecular differences between the two pro-N-cadherin bands. To limit the factors that may modify the apparent molecular weight of pro-N-cadherin, we created a noncleavable N-cadherin mutant (FXa-N-cadherin-ST) in which the furin motif was replaced by a factor-Xa site (similar in size but not cleavable in the cell; Fig. S3 C). As expected, this mutant generated two pro-N-cadherin bands in the chicken NT but no mature N-cadherin (Fig. S3 D). Interestingly, treating purified FXa-N-cadherin-ST either with EndoH that removes only immature glycosylation or with PNGase that removes immature and mature glycosylation decreased the apparent molecular weight of both pro-N-cadherin bands (Fig. 5, C and D; the upper and lower pro-N-cadherin bands are indicated by blue and purple arrows, respectively). By contrast, dephosphorylation (AP treatment) converted the two bands into one (purple arrow), indicating that the molecular weight difference between the two pro-N-cadherin bands was due to phosphorylation (Fig. 5 E). Combining β-catenin expression with dephosphorylation, we identified up to four different forms of N-cadherin, corresponding to phosphorylated and unphosphorylated forms of pro-N-cadherin and mature N-cadherin, with β-catenin expression promoting the conversion of phospho-pro-N-cadherin into phospho-N-cadherin (Fig. 5, F and G). Moreover and irrespective of β-catenin expression, N-cadherinΔβCat·ST was purified mostly as an unphosphorylated pro-N-cadherin (Fig. 5, H and I), and interestingly, β-catenin only associated with the phosphorylated form of pro-N-cadherin (Fig. 5 J). Hence, β-catenin appears to bind directly to pro-N-cadherin to promote its conversion into mature N-cadherin. Indeed, pro-N-cadherin processing was stimulated similarly by β-cateninΔC, a mutant β-catenin with no transcriptional activity (Valenta et al., 2011) but with structural properties equivalent to the wild-type β-catenin (Fig. 5 K and Fig. S3 E).

Dbnl is required for N-cadherin maturation

Having shown that β-catenin drives pro-N-cadherin conversion to mature N-cadherin, we searched for proteins that interact
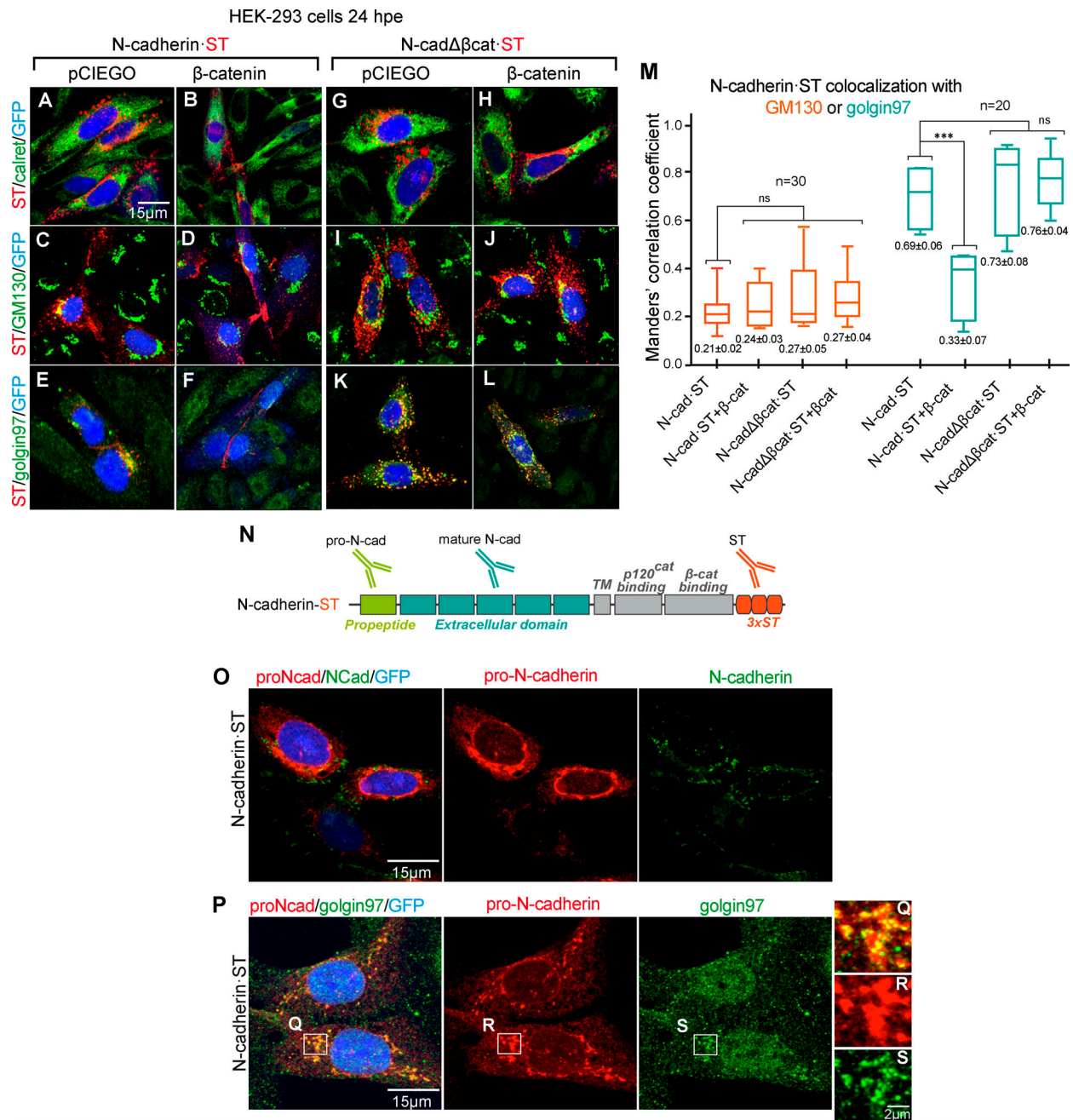
Figure 4. β-catenin deficiency induces pro-N-cadherin accumulation in the TGN. (A–L) HEK-293 cells transfected with N-cadherin (A–F) or N-cadherinΔβcat (G–L), plus the control vector or β-catenin, and stained with anti-N-cadherin (red) and an ER (calreticulin), Golgi (GM130), or trans-Golgi/TGN (Golgin97) marker in green. Nuclear GFP expression indicative of transfection is shown in blue. **(M)** Box plot showing the Manders correlation coefficients for N-cadherin and GM130 (red boxes; n = 30) or Golgin97 (blue boxes; n = 20) calculated from cultures in A–L. Each experimental condition was compared with every other experimental condition using a one-way ANOVA with Tukey's multiple comparisons test. **(N)** Scheme of the regions of N-cadherin targeted by the antibodies used. **(O)** HEK-293 cells transfected with N-cadherin, stained with anti-pro-N-cadherin (red) and anti-N-cadherin (green). The nuclear GFP expression indicative of transfection is shown in blue. **(P)** Same transfection as in O, stained with anti-pro-N-cadherin (red) and anti-Golgin97 (green). **(Q–S)** Areas amplified from P. ***, P < 0.001. cad, cadherin; TM, transmembrane domain.

with N-cadherin but not with N-cadherinΔβcat (Fig. 6 A). We transfected ST-tagged forms of both molecules in HH12 chicken NTs, and after 24 h at HH18, the transfected areas were dissected, mildly cross-linked, and homogenized. We used Strep-Tactin columns to purify the proteins associated to N-cadherin·ST or N-cadherinΔβcat·ST, and after reverting the crosslinking, we

studied their identity by liquid chromatography-mass spectrometry (LC-MS). We identified a total of 488 proteins, 63 only associating with N-cadherin, 67 only with N-cadherinΔβcat, and 358 with both (Fig. 6 B and Table S1). Among the 63 proteins that interacted with N-cadherin but not with N-cadherinΔβcat, new (37%) and known (63%) interactions were detected. Using an online service (Binder
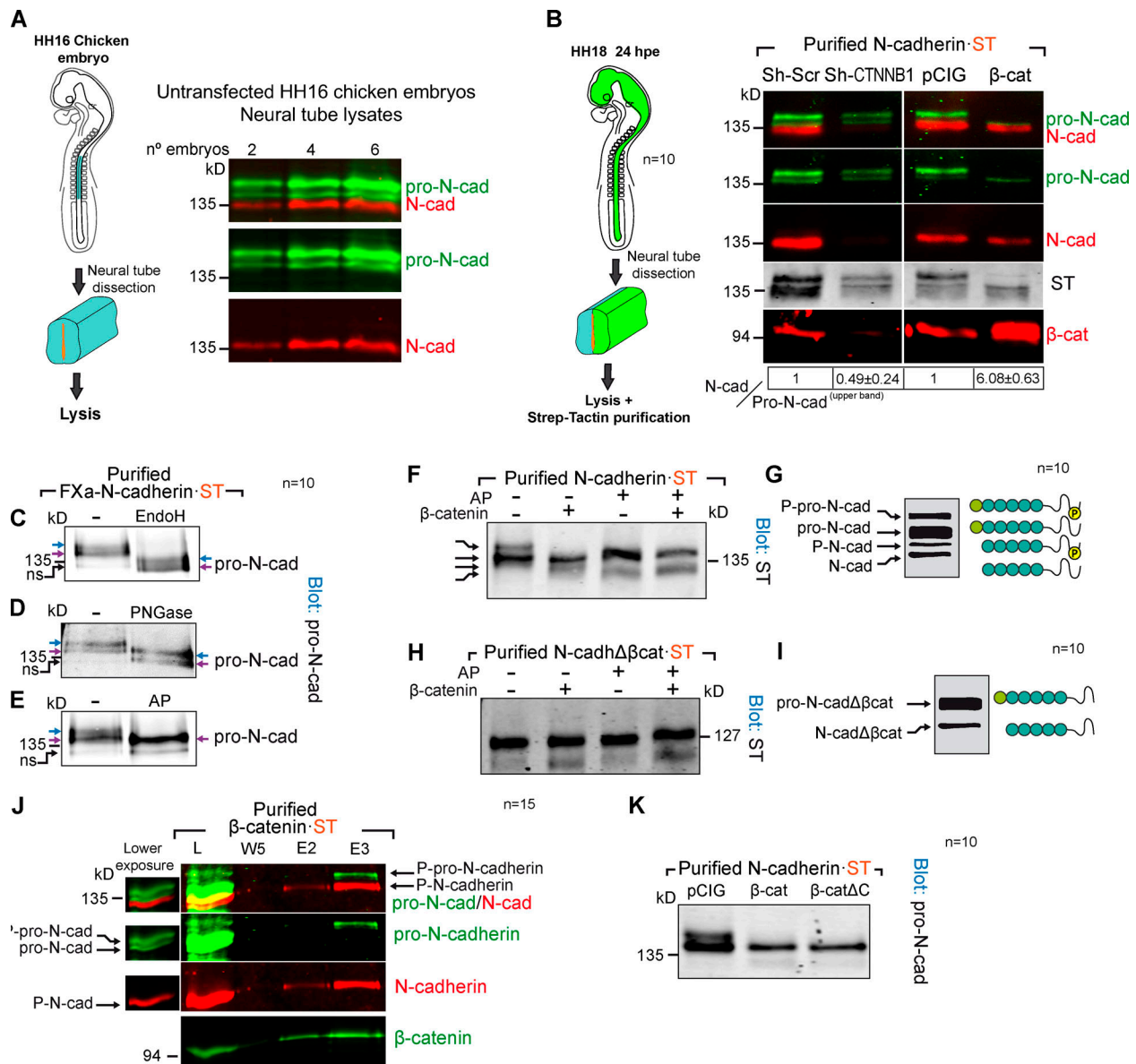
Figure 5. **β-catenin binds phosphorylated pro-N-cadherin, promoting its conversion into mature N-cadherin. (A)** Western blot of whole lysates from untransfected HH16 chicken embryos probed with antibodies against pro-N-cadherin (green) and N-cadherin (red). **(B)** Western blot of Strep-Tactin–purified N-cadherin-ST electroporated for 24 h into HH12 chicken NTs with Sh-CTNNB1 or β-catenin and dissected at HH18. The blot was probed with antibodies against pro-N-cadherin (green), N-cadherin (red), ST (gray) and β-catenin (red). The N-cadherin/pro-N-cadherin[upper band] ratios normalized to the transfection controls (considered 1) are shown at the bottom of each lane ($n = 10$). **(C–E)** Western blot of Strep-Tactin–purified FXa-N-cadherin-ST electroporated into HH12 chicken NTs and dissected 24 h later at HH18 and treated with EndoH (C; degrades immature N-linked glycosylation), PNGase (D; degrades all N-linked glycosylation), or AP (E; AP, dephosphorylates). The blots were probed with antibodies against pro-N-cadherin. The two pro-N-cadherin bands are labeled with blue and purple arrows. After AP treatment, the two bands turn into one; the lower one is labeled with a purple arrow. The presence of a nonspecific band is labeled as ns ($n = 10$). **(F)** Blot of Strep-Tactin–purified fractions of HH18 chicken NTs 24 hpe with N-cadherin-ST, with or without β-catenin, and treated with AP ($n = 10$). **(G)** A scheme of the proposed molecular nature of each band observed in F. **(H)** Same experiment as in F but with N-cadherinΔβcat ($n = 10$). **(I)** A scheme of the proposed molecular nature of each band observed in H. **(J)** Western blot of Strep-Tactin–purified fractions from HH18 chicken NTs 24 hpe with β-catenin·ST and probed with antibodies against pro-N-cadherin (green), N-cadherin (red), and β-catenin (green). A weaker exposure of the lysate lane is shown to the left of the main panel. Note that only the upper pro-N-cadherin band binds to β-catenin·ST ($n = 15$). **(K)** Experiment as in B but comparing the transfection of β-catenin to β-cateninΔC, a β-catenin mutant with no transcriptional activity. Numeric data are expressed as the mean ± SD ($n = 10$). cad, cadherin; E, elution; L, lysate; Scr, scramble; W, wash.

et al., 2014), we studied the subcellular distribution of these 63 proteins (Fig. 6 B and Table S2). Because we were interested in proteins involved in N-cadherin maturation and transport to the AC, we transfected HH12 chicken embryos to knock down each of the seven proteins predicted to be located in the Golgi

apparatus, and we then studied the levels of pro-N-cadherin and mature N-cadherin at HH18 (Fig. S4, A and B). Notably, the knockdown of DBNL, an SH3-containing actin-binding protein that is located in endosomes and the Golgi apparatus (Fucini et al., 2002; Le Bras et al., 2004), increased the pro-N-
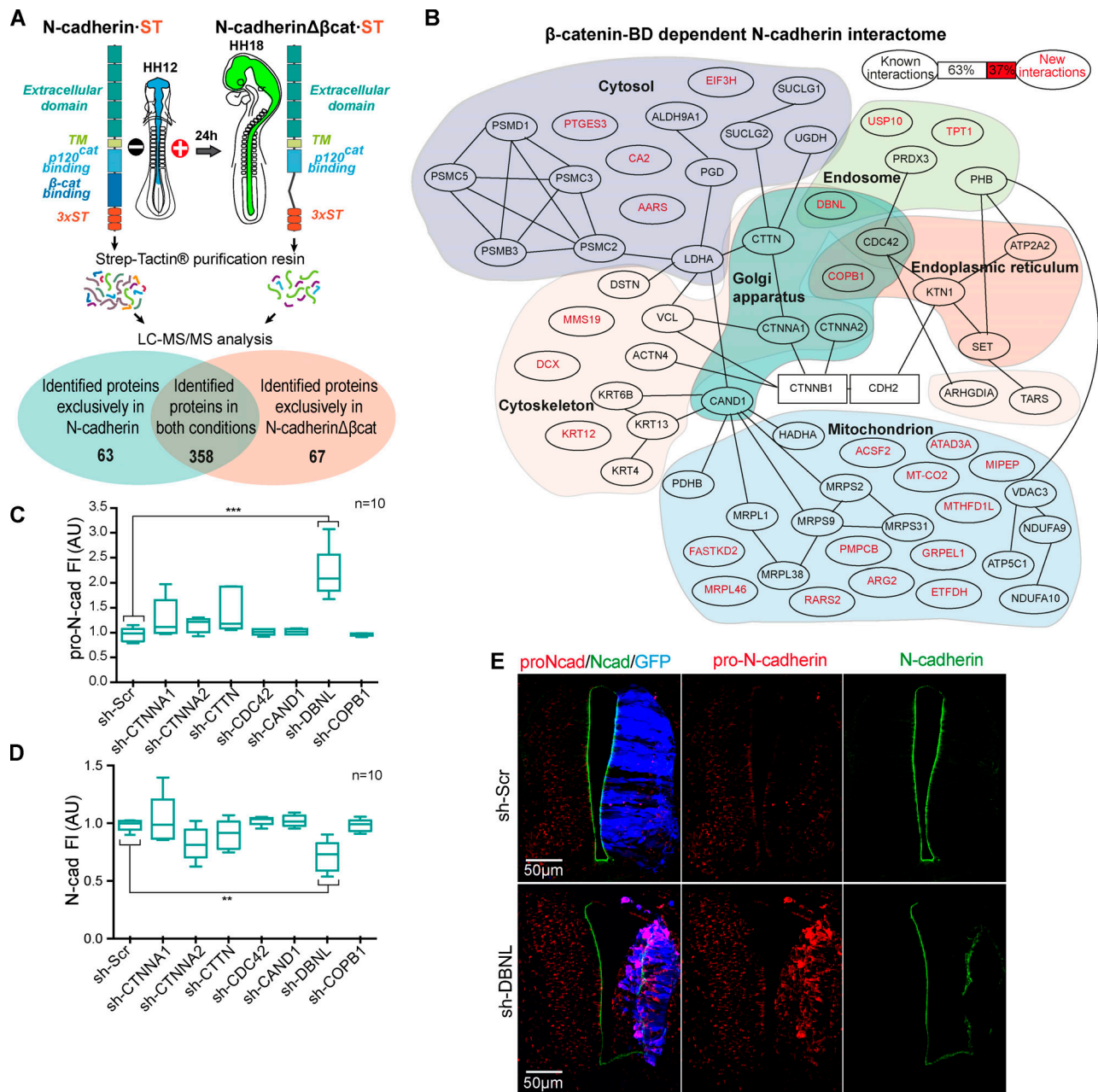
Herrera et al.
Dbnl and β-catenin promote N-cadherin maturation

Journal of Cell Biology   9 of 19
https://doi.org/10.1083/jcb.202007055

Figure 6.   **Discovery of new β-catenin–dependent interactions with N-cadherin implicated in its maturation. (A)** Scheme of the procedure followed to find new β-catenin–dependent interactions with N-cadherin. **(B)** The 63 proteins found in N-cadherin but not in N-cadherinΔβcat purification were assigned to subcellular compartments. The new (red) and known (black) interactions are shown, and known interactions are indicated by black lines in the tree. **(C and D)** Levels of pro-N-cadherin and N-cadherin, measured in HH23 chicken NTs transfected for 48 h with shRNAs targeting the proteins predicted to be located in the Golgi. Each experimental condition was compared with the respective control using a one-way ANOVA with a Dunnett's multiple comparisons test (n = 10). **(E)** DBNL knockdown stained with antibodies against pro-N-cadherin (red) and N-cadherin (green). The GFP denoting transfection is shown in blue. **, $P < 0.01$; ***, $P < 0.001$. cad, cadherin; FI, fluorescence intensity; MS/MS, tandem mass spectrometry; Scr, scramble; TM, transmembrane domain; BD, binding domain.

cadherin and reduced the mature N-cadherin detected, this being the only protein knockdown that caused significant changes in either pro or mature N-cadherin expression (Fig. 6, C and D). In addition, it caused tissue alterations that included ventricle invasion (Fig. 6 E) and a loss of apico-basal polarity (mislocation of N-cadherin, β-catenin, and aPKC; Fig. 6 E and Fig. S5 A).

Interestingly, Dbnl was recently shown to control neuronal migration by regulating N-cadherin expression on plasma membrane in the developing cerebral cortex (Inoue et al., 2019). In the NT, Dbnl was localized widely in the Golgi region and in the space between the Golgi and the AC (Fig. 7 A). However, DBNL knockdown caused pro-N-cadherin accumulation, mostly around the nucleus and in the Golgi region (Fig. 7 B). These
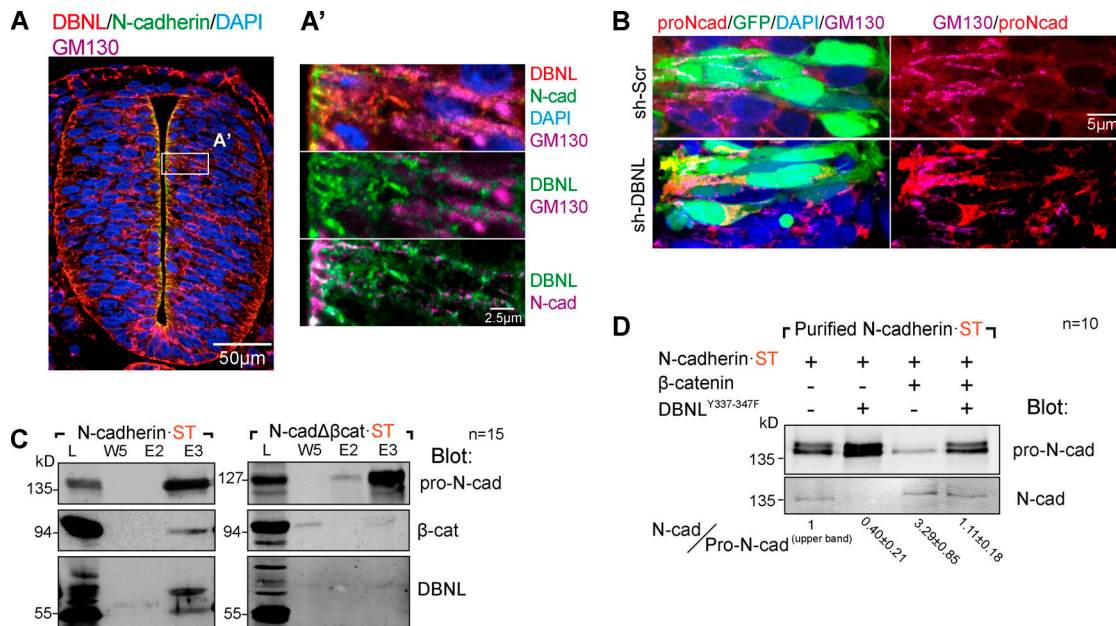
Figure 7. **Dbnl is required for N-cadherin maturation. (A)** Untransfected HH16 chicken NT section stained with antibodies against Dbnl (red), N-cadherin (green), and GM130 (purple). DAPI shows the nucleus in blue. The area labeled as A' is amplified in the right panels in which the relevant channels are shown two by two to reveal colocalization. **(B)** Higher magnification images of NTs transfected with control shRNA or sh-DBNL and stained with antibodies against pro-N-cadherin (red) and GM130 (purple). GFP (green) indicates transfection, and DAPI (blue) shows the nuclei. **(C)** Western blot of Strep-Tactin–purified N-cadherin-ST or N-cadherinΔβcat·ST electroporated into HH12 chicken NTs and dissected at HH18 24 h later. The blots were probed with antibodies against pro-N-cadherin, β-catenin, and Dbnl (n = 15). **(D)** Western blot of Strep-Tactin–purified N-cadherin·ST 24 h after electroporation into HH12 chicken NTs with DBNL[Y337-347F], β-catenin, or both and dissected at HH18. The blot was probed with antibodies against pro-N-cadherin and N-cadherin. The N-cadherin/pro-N-cadherin[upper band] ratios normalized to the transfection controls (considered as 1) are shown at the bottom of each lane. Numeric data are expressed as the mean ± SD (n = 10). cad, cadherin; Scr, scramble.

results strongly suggest that the lack of Dbnl severely delayed N-cadherin maturation, thereby blocking its transportation to the AC. Notably, all these effects were very similar to those obtained following N-cadherinΔβcat transfection.

In accordance with the MS results, Dbnl was detected in Western blots of purified N-cadherin·ST but not N-cadherinΔβcat·ST (Fig. 7 C). We detected Dbnl as 55- and 70-kD isoforms, which corresponded to two different phosphorylation states (Fig. S5, B and C). Phosphorylation of the DBNL aa residues Y337 and Y347 is required for its activity, and indeed, a mutant DBNL (DBNL-2F) in which these two residues were mutated to phenylalanine demonstrated a strong dominant negative activity, reducing N-cadherin expression on the plasma membrane in the cerebral cortex (Inoue et al., 2019). Therefore, we wondered whether the influence of β-catenin on pro-N-cadherin maturation was affected by DBNL-2F. We transfected HH12 chicken embryos with N-cadherin·ST plus DBNL-2F, β-catenin, or both; 24 h later (HH18), the embryos were dissected and lysed, and N-cadherin-ST was purified on Strep-Tactin columns. As usual, ST-containing proteins eluted mostly in fraction 3, and thus, we used this fraction to calculate (as in Fig. 5 B) the N-cadherin/pro-N-cadherin[upper band] ratio. As expected, DBNL-2F expression induced pro-N-cadherin accumulation (ratio = 0.40 ± 0.21), and whereas β-catenin incremented the amount of mature N-cadherin over pro-N-cadherin (ratio = 3.29 ± 0.85), the effect of β-catenin disappeared when DBNL-2F was also transfected (ratio = 1.11 ± 0.18; Fig. 7 D). Thus, β-catenin and Dbnl both promote the

processing of N-cadherin, and it would appear that the interaction of Dbnl with N-cadherin is mediated by β-catenin.

The persistence of pro-N-cadherin induces a loss of apico-basal polarity, causing aberrant delamination, a breach of the basal membrane, and mesenchymal invasion

The data so far have demonstrated that β-catenin and Dbnl are required for pro-N-cadherin conversion into mature N-cadherin and that a deficit of β-catenin or Dbnl disrupts the apico-basal polarity of the neuroepithelium. To study the consequences pro-N-cadherin persistence, we used FXa-N-cadherin, a variant that cannot produce mature N-cadherin (Fig. S3 D) but that can still bind to and repress β-catenin transcriptional activity in a similar way to N-cadherin (Fig. S3, D and F). In neural progenitors, transfected N-cadherin generated pro-N-cadherin that accumulated around the nucleus and along the apical process and N-cadherin that accumulated along the apical process and in the AC (Fig. 8 A, arrows). Upon delamination, an apical-to-basal translocation of the Golgi apparatus takes place in neurons (Taverna et al., 2016), and thus in delaminated neurons, the NT pro- and mature N-cadherin were both observed basal to the nucleus (Fig. 8 A, arrowheads). However, FXa-N-cadherin transfection increased the pro- but not the mature N-cadherin (Fig. 8, C and D). Notably, in contrast to N-cadherin transfection where cell shape and epithelium structure were normal (Fig. 8, A and F), cells transfected with FXa-N-cadherin were round, with no apparent apico-basal polarity, and they frequently
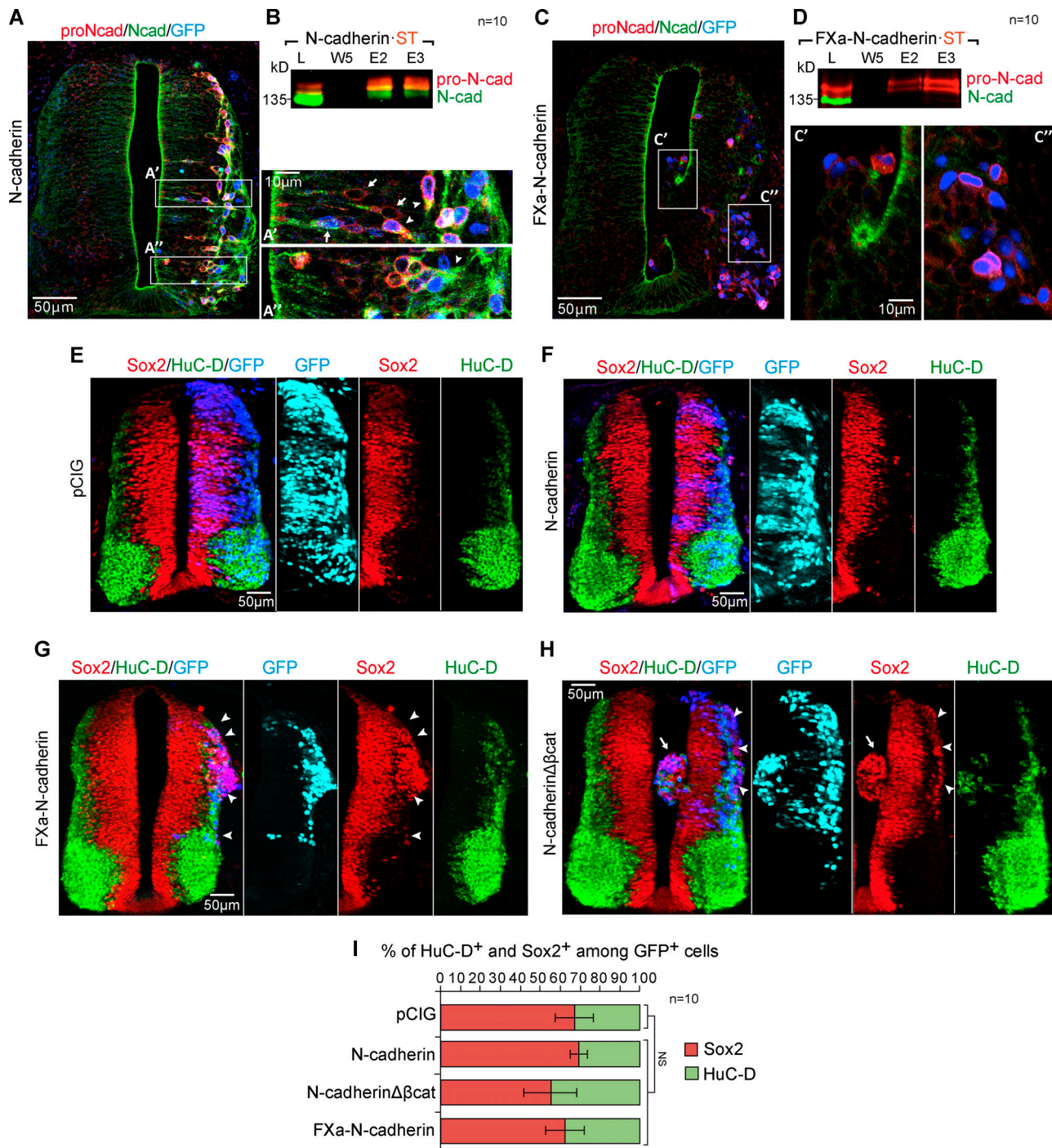
Figure 8. **The persistence of pro-N-cadherin induces a loss of apico-basal polarity, causing aberrant delamination, ventricle invasion, and basal membrane rupture. (A)** HH23 chicken NTs 48 hpe with N-cadherin and probed with antibodies against pro-N-cadherin (red) and N-cadherin (green) and with nuclear GFP indicating transfection (blue). The areas labeled as A' and A'' are amplified on the right, and the arrows indicate neural precursors, while the arrowheads show the delaminated neurons. **(B)** Western blot of Strep-Tactin–purified fractions from HH18 chicken NTs 24 hpe with N-cadherin·ST probed with antibodies against pro-N-cadherin (red) and N-cadherin (green); $n = 10$. **(C and D)** A similar experiment as that shown in A and B but using FXa-N-cadherin·ST ($n = 10$). **(E–H)** HH23 chicken NTs 48 hpe with control, N-cadherin, FXa-N-cadherin, or N-cadherinΔβcat and stained with antibodies against Sox2 (red) and HuC/D (green). Nuclear GFP expression indicates transfection (blue or cyan in the split channel composition). In panel G, the arrowheads indicate Sox2+ cells occupying the mantle zone. In panel H, the arrowheads indicate Sox2+ cells occupying the mantle zone and the arrow a mass of Sox2+ cells invading the ventricle. **(I)** Bar graph showing the mean ± SD of the Sox2+ and HuC/D+ cells among the transfected population. Each experimental condition was compared with the respective control using a one-way ANOVA with a Dunnett's multiple comparisons test ($n = 10$). cad, cadherin; E, elution; L, lysate; W, wash.

Herrera et al.
Dbnl and β-catenin promote N-cadherin maturation

Journal of Cell Biology 12 of 19
https://doi.org/10.1083/jcb.202007055

invaded the ventricle and/or the mesenchyme (Fig. 8, C and G). β-Catenin activity enhances neural precursor stemness, preventing differentiation (Herrera et al., 2014), whereas β-catenin recruitment to AJs by E-cadherin represses cell growth and transformation (Gottardi et al., 2001; Stockinger et al., 2001). Thus, because pro-N-cadherin binds β-catenin but AJs do not form, we wondered whether pro-N-cadherin affects the differentiation of neural precursors. Significantly, FXa-N-cadherin did not change the ratio between neural progenitors and neurons (Fig. 8, G and I), but rather, it induced a significant ectopic accumulation of progenitors in the mantle zone (Fig. 8 G, arrowheads). Interestingly, transfection of N-cadherinΔβcat, the N-cadherin mutant that does not bind β-catenin and that mostly remains as pro-N-cadherin, caused a similar ectopic accumulation of precursors (Fig. 8 H, arrowheads). Thus, the presence of pro-N-cadherin disrupts apico-basal polarity independently of β-catenin activity. In summary, a failure in N-cadherin maturation disrupts the formation of AJs, on the one hand, weakening the apical surface of the neuroepithelium and provoking invasion of the ventricle and on the other hand, triggering the premature delamination of neural precursors that accumulate in the mantle zone and invade the surrounding mesenchyme.

Discussion

β-catenin binding promotes pro-N-cadherin processing and transport to the AC

We previously demonstrated that stable forms of β-catenin induce oversized ACs containing abnormally large amounts of N-cadherin, β-catenin, actin, and active aPKC. In addition, we also showed that that β-catenin induces both the transcription and the recruitment of aPKC to the ACs, and we demonstrated that the hyperpolarization induced by β-catenin disappeared with the transfection of a dominant negative form of aPKCι. Moreover, we found that the depolarization of the neuroepithelium induced by aPKMz, an active form of aPKC, could be reverted by β-catenin, which concentrated all the aPKC activity in the AC and prevented its ectopic activation in the basolateral compartment (Herrera et al., 2014). Accordingly, we wondered whether N-cadherin, β-catenin, and aPKC themselves formed a complex and, if so, whether this complex was formed at the AC or was preassembled and transported there.

We demonstrate here that aPKC colocalizes with N-cadherin or β-catenin exclusively at the AC of NSCs, whereas N-cadherin also colocalizes with β-catenin in the Golgi apparatus, albeit less intensely than in the AC. Nevertheless, the exact point at which the cadherin/β-catenin complex is initially established remains unclear. It was first demonstrated that β-catenin binds to E-cadherin early in the biosynthetic pathway (Hinck et al., 1994), and later, it was proposed that the E-cadherin/β-catenin complex was formed in the ER. Indeed, the formation of this complex allowed efficient ER exit and basolateral membrane targeting of a chimeric protein that contains the cytoplasmic domain of E-cadherin in polarized MDCK cells (Chen et al., 1999). In addition, β-catenin was seen to bind to PX-RICS, a GTPase-activating protein for Cdc42 that associates with dynein-dynactin, promoting ER-to-Golgi transport of the N-cadherin/β-catenin

complex. Indeed, the accumulation of the N-cadherin/β-catenin complex in the ER as a result of PX-RICS downregulation leads to a decrease in cell adhesion (Nakamura et al., 2010; Nakamura et al., 2008). Alternatively, in vitro studies demonstrated that β-catenin presents an ∼800-fold higher affinity for E-cadherin when this is phosphorylated (McEwen et al., 2014) and that the β-catenin/E-cadherin complex forms before the excision of the propeptide domain of E-cadherin (Wahl et al., 2003). Therefore, we assume that pro-cadherins are phosphorylated before they bind tightly to β-catenin, and indeed, we found that only the phosphorylated form of pro-N-cadherin could be purified with β-catenin.

Although the compartment in which pro-cadherins are phosphorylated is unknown (McEwen et al., 2014), the phosphorylated pro-N-cadherin can be effectively deglycosylated by EndoH, an endoglycosidase that only acts on high-mannose immature glycosylation (found in the ER and cis-Golgi apparatus). Hence, pro-N-cadherin phosphorylation and binding to β-catenin must take place before entry into the medial/trans-Golgi compartment. Here, we show that N-cadherin and β-catenin colocalize more in the post-Golgi space than in the Golgi apparatus itself, reaching a maximum in the AC. However, the rat monoclonal anti-N-cadherin antibody used in the colocalization experiments preferentially detects mature N-cadherin over pro-N-cadherin. Therefore, this observation reconciles our colocalization results with previous results demonstrating that pro-N-cadherin is phosphorylated in the ER/Golgi where it binds with high affinity to β-catenin.

E-cadherin mutants that cannot bind to β-catenin have consistently been reported to accumulate in intracellular compartments, including the TGN (Miyashita and Ozawa, 2007). Although interestingly, we observed that N-cadherinΔβcat, a mutant construct that lacks the β-catenin–binding domain and, consequently, the main phosphorylation sites, does not accumulate in the ER but, rather, accumulates as pro-N-cadherin in Golgin97 vesicles in the TGN. Likewise, pro-N-cadherin does not need to be coupled to β-catenin to leave the ER or to reach the TGN, but conversely, the lack of β-catenin prevents the excision of the propeptide and causes pro-N-cadherin to accumulate in the TGN.

We now describe a new β-catenin–dependent interaction between N-cadherin and Dbnl, a Golgi-localized actin-binding protein. Dbnl is specifically regulated by the coat-binding domain of the vesicle cargo protein p23, and it is involved in anterograde protein trafficking to the Golgi (Fucini et al., 2002). A recent report showed that Dbnl upregulates the amount of N-cadherin protein at the neuronal plasma membrane of differentiating cortical neurons (Inoue et al., 2019). Indeed, we found that Dbnl knockdown leads to pro-N-cadherin accumulation and, similarly, the N-cadherin mutant lacking the β-catenin–binding domain that fails to cleave the propeptide accumulates as pro-N-cadherin. Dbnl binds simultaneously to F-actin and to components of the Golgi vesicular system, whereas while β-catenin does not bind directly to F-actin, it interacts with the actin cytoskeleton through actin-binding proteins like α-catenin and vinculin. Moreover, Dbnl forms β-catenin–dependent complexes with N-cadherin, and notably, both Dbnl and β-catenin deficiency impairs pro-N-cadherin

processing. Thus, β-catenin may promote pro-N-cadherin processing by recruiting vesicular components that are associated to F-actin through Dbnl.

In contrast to the long-distance association observed between N-cadherin and β-catenin, colocalization of aPKC with either N-cadherin or β-catenin occurs almost exclusively in the AC. Our results demonstrate that N-cadherin/β-catenin complexes and aPKC are delivered separately to the AC, yet no apical aPKC accumulation was observed in the absence of N-cadherin/β-catenin. aPKC reaches the apical membrane as part of a complex containing Par3 and Par6, and there, the combined activity of Cdc42 and PDK1 activates the kinase activity of aPKC, which like β-catenin and N-cadherin is required to maintain apico-basal polarity (Chen and Zhang, 2013). Therefore, although more evidence will be required to fully demonstrate our model, we speculate that the boundary region between the apical and subapical domains where the three molecules coexist serves as a docking station where β-catenin interacts with Par3 through its PDZ binding domain (Gujral et al., 2013), capturing Par3/Par6/aPKC complexes that are then shunted to the apical membrane.

Does β-catenin tumor suppressor activity rely on its capacity to promote pro-N-cadherin processing?

Wnt-type medulloblastoma (MB) is mainly caused by stable forms of β-catenin, and it is the least aggressive of the four types of MBs mainly due to its low invasiveness and the fact that it rarely metastasizes. Notably, the expression of β-catenin significantly increases survival in a mouse model of Shh-type MB (Pöschl et al., 2014), which indicates that β-catenin acts simultaneously as both an oncogene and a tumor suppressor. Very recently, using single-cell RNA sequencing technology, the presence of rare Wnt-active cells in non-Wnt human MBs was demonstrated (Manoranjan et al., 2020). These cells not only retain the impaired tumorigenic potential of Wnt-type MB but also are believed to be responsible for the inhibition of tumor growth caused by activation of the ectopic Wnt pathway in non-Wnt MB xenografts. Among the multiple changes that occur during the development of invasive malignancies (Hanahan and Weinberg, 2000), two major events are the onset of uncontrolled cell proliferation and the loss of cell adhesion, together driving the invasion of local tissues (Birchmeier et al., 1996). E-cadherin is considered a suppressor of invasion because it increases cell adhesion in epithelial tissues (Gumbiner, 2000; Larue et al., 1996) and binds to β-catenin and prevents its transforming activity (Gottardi et al., 2001; Jeanes et al., 2008). Indeed, epithelia that express E-cadherin strongly are more resistant to transformation by oncogenic mutations of β-catenin (Huels et al., 2015). We show here that mutations that prevent pro-N-cadherin processing induce a loss of polarity, ventricle invasion, premature delamination, ectopic progenitor accumulation in the mantle zone, and a breach of the basal membrane that leads to the invasion of the surrounding mesenchyme. It is significant that a cytoplasmic (perinuclear) rather than cell-surface distribution of E-cadherin has often been reported in carcinoma cells, suggesting that the transport of E-cadherin to the cell surface is impaired in some carcinomas (Carpenter et al.,

2002). Moreover, the expression of surface pro-N-cadherin in melanoma and glioblastoma cell lines promotes tumor cell invasion, and a positive ratio of pro-N-cadherin/N-cadherin correlates with increased malignancy in different human cancers (Maret et al., 2010). In addition, pro-N-cadherin has been detected on the cell surface of a highly invasive subpopulation of triple-negative breast tumor cells (Nelson et al., 2016). Together, these data indicate that the loss of adhesiveness caused by pro-N-cadherin at the cell surface may have an accumulative effect on the oncogenic capacity of other oncogenes, as occurs with β-catenin.

Although pro-N-cadherin binds to and represses β-catenin transcriptional activity in a similar way to N-cadherin, accumulation of pro-N-cadherin but not of N-cadherin induces the invasion of the mesenchyme surrounding the NT; therefore, we have to assume that it is the loss of polarity caused by pro-N-cadherin that actually promotes the invasive phenotype. Thus, we propose that β-catenin tumor suppressor activity relies on its ability to promote the maturation of pro-N-cadherin, with the consequent formation of larger AJs. This effect would not only strengthen cell adhesion but also restrict the delamination and dissemination of tumor cells.

Materials and methods

Commercial antibodies and chemicals

The following antibodies and reagents were used in these studies: Mouse antibodies against HuC/D (#A21271, 1:500; Molecular Probes), β-catenin (#C7207, 1:200; Sigma), β-catenin (#9562, 1:500; Cell Signaling Technologies), Golgin97 (#A21270, 1:100; Invitrogen), Strep-tag (#2-1507-001, 1:500; IBA Lifesciences), CLIMP63 (#C5840-93, 1:1,000; United States Biological), aPKCζ/λ (#SC-17781, 1:200; Santa Cruz Biotechnology), GM130 (#610822, 1:500; BD Biosciences), rat antibodies against N-cadherin (#13-2100, 1:200; Invitrogen), rabbit antisera against Sox2 (#48-1400, 1:500; Invitrogen), calreticulin (#ab2907, 1:1,000; Abcam), and the chemicals rhodamine-phalloidin (#R415, 1:250; Invitrogen).

In-house antisera

The rabbit antisera used to detect FLAG and RFP were described previously (Herrera et al., 2014), while the pro-N-cadherin antiserum was raised against a GST fusion protein with the propeptide region of chicken N-cadherin (aa 29–164).

DNA constructs

Proteins were expressed using the pCIG (Megason and McMahon, 2002; Niwa et al., 1991), pCIEGO, pIRES, or pCS2 vectors, and inhibitory shRNAs were generated with pSHIN (Kojima and Borisy, 2014). To generate ST-tagged proteins, three copies of the Strep-tag II peptide (WSHPQFEK) were added to the C-terminus of the proteins indicated. Canonical Wnt activity was evaluated with TOPFlash luciferase reporter (Staal et al., 1999). Deletion and substitution mutants were generated through standard techniques, and all the constructs were sequenced before use.

Vectors

The following vectors were used: pCIG (chicken β-actin promoter/cytomegalovirus [CMV]-IE enhancer, EGFP-expressing bicistronic vector), pCIEGO (pCIG with no IRES-EGFP), pIRES (bicistronic human CMV-IE promoter/enhancer, EGFP-expressing vector), pCS2 (simian CMV-IE94 promoter), and pSHIN (expresses inhibitory shRNAs driven by the human H1 promoter and EGFP driven by the artificial SRα promoter).

pCIG constructs

The following constructs were cloned in pCIG: chicken N-cadherin; N-cadherin·ST, ST-tagged chicken N-cadherin; N-cadherinΔβcat, chicken N-cadherinΔ844–912; N-cadherinΔβcat·ST, ST-tagged chicken N-cadherinΔ844–912; XFa-N-cadherin, the furin consensus cleavage sequence (LKRQKRDW) aa 159–166 of chicken N-cadherin substituted by the factor Xa cleavage sequence (LKIEGRDW); FXa-N-cadherin·ST, ST-tagged chicken FXa-N-cadherin; sβ-catenin, human β-catenin-S33Y; sβ-catenin·ST, ST-tagged human β-catenin-S33Y; sβ-cateninΔC, human β-catenin-S33Y-Δ674–782; aPKCι·ST, ST-tagged human aPKCι; Tcf3-VP16, HMG box of mouse TCF3 fused to the VP16 transcriptional activator (Kim et al., 2000); and DBNL-Y337-347F (Inoue et al., 2019; Niwa et al., 1991).

pCIEGO construct

The following construct was cloned in pCIEGO: sβ-Catenin (human β-catenin-S33Y).

pIRES construct

The following construct was cloned in pIRES: human furin (Maret et al., 2012).

pCS2 constructs

The following constructs were cloned in pCS2: N-cadherin·GFP, chicken N-cadherin with EGFP fused to the C-terminus; membrane-targeted GFP (mbGFP), GFP with glycosylphosphatidylinositol fused to the C-terminus; mbRFP, RFP with glycosylphosphatidylinositol fused to the C-terminus

pSHIN constructs

To produce inhibitory shRNA targeting the following chicken genes: *CAND1* (5′-CGCCCTCTCCTCCTTCTCT-3′), *CDC42* (5′-CTT CTGCAAAGCTGGTGTT-3′), *COPB1* (5′-GTCCCTCTCTCATATGCT G-3′), *CTNNA1* (5′-ATGGCCTCGCTCAACCTCC-3′), *CTNNA2* (5′-ATGGCAGACTCCTCGTGCA-3′), *CTNNB1* (5′-ATCCCAGAACTG ACCAAAC-3′), *CTTN* (5′-AAGAACAGGAAGACCGAAG-3′), *DBNL* (5′-GAATCAGTGGAGAAAGCCC-3′), Scrambled (5′-CCGGTC TCGACGGTCGAGT-3′).

Chicken embryo in ovo electroporation

Eggs from white Leghorn chickens were incubated at 37.5°C in an atmosphere of 45% humidity, and the embryos were staged according to Hamburger and Hamilton (1992). Chicken embryos were electroporated with column-purified plasmid DNA (1–2 µg/µl) in H_2O containing Fast Green (0.5 µg/µl). Briefly, plasmid DNA was injected into the lumen of HH12 NTs; electrodes were placed on either side of the NT, and electroporation was performed by applying five 50-ms square pulses using an INTRAcel

Dual Pulse (TSS10) electroporator set at 25 V. Transfected embryos were allowed to develop to specific stages and then dissected under a fluorescence dissection microscope. In our conditions, HH12 embryos electroporated for 24 and 48 h normally reached stages HH18 and HH23, respectively. Embryos that did not develop to the expected stages were discarded. To stage the different embryos, we used the staging guide previously published (Hill, 2021).

Purification of Strep-tag II–tagged proteins on Strep-Tactin columns

We optimized the previously described methods to purify proteins carrying ST tags and their interacting partners (Klockenbusch and Kast, 2010; Kubben et al., 2010), an approach that permitted the detection of mild and/or transitory interactions. Strep-tag II is a short peptide (8 aa; WSHPQFEK) that binds with high affinity/selectivity to Strep-Tactin, an engineered streptavidin. To tag proteins with Strep-tag, three copies of the Strep-tag peptide were inserted at the C-terminus of the selected proteins. For purification experiments, chicken embryos or cell cultures electroporated for 24 h with tagged proteins were dissolved in the following buffer: 20 mM Tris-HCl (pH 7.4), 137 mM NaCl, 10% glycerol, 1% NP-40, 1 mM $CaCl_2$, 1 mM $MgCl_2$, 10 µg/ml aprotinin, 10 µg/ml leupeptin, and 1 mM PMSF, with 1 ml of buffer used for each 10-cm culture dish or 15 embryos (HH18 embryos). For copurification experiments, GFP⁺ areas of the electroporated NTs were dissected out in cold PBS, and then the protein complexes were mildly cross-linked with 1% formaldehyde for 10 min at room temperature. The crosslinking reaction was stopped with glycine (up to 125 mM), and the cross-linked embryos were then dissolved by sonication (2 × 30 s at 10-µm amplitude) in ice-cold SDS lysis buffer (1% SDS, 10 mM EDTA, 50 mM Tris-HCl [pH 8.1], 10 µg/ml aprotinin, 10 µg/ml leupeptin, 1 mM PMSF, 5 mM NaF, and 1 mM NaVa). The protein samples were diluted in a dilution buffer (1.1% Triton X-100, 1.2 mM EDTA, 17 mM Tris-HCl [pH 8.1], 170 mM NaCl, 10 µg/ml aprotinin, 10 µg/ml leupeptin, 1 mM PMSF, 5 mM NaF, and 1 mM NaVa) to a final concentration of 0.1% SDS, 0.1% Triton X-100, 2 mM EDTA, 20 mM Tris-HCl (pH 8.1), 150 mM NaCl, 10 µg/ml aprotinin, 10 µg/ml leupeptin, 1 mM PMSF, 5 mM NaF, and 1 mM NaVa. In these experiments, the insoluble material was removed by centrifugation at 18,500 ×*g* for 5 min, and purification was performed on prepacked Strep-Tactin (0.2-ml bed volume [bv] Gravity Flow Superflow® columns, #2-1209-550; IBA Lifesciences) following the manufacturer's instructions and using the reagents provided with the columns, adding 1% Triton X-100 (purifications) or 1% Triton X-100 and 0.1% SDS (copurifications) to the wash and elution buffers. Briefly, columns were prestabilized with 5 bv of lysis buffer, and 1 ml of lysate was applied to each 0.2-ml column, washed with 5–15 bv, and finally eluted in 100 µl aliquots. Purified proteins were stored at –80°C for further use.

Protein identification (LC-tandem MS)

SDS band gels were washed with ammonium bicarbonate (NH₄HCO₃ 25 mM) and acetonitrile (ACN), and immediately, the samples were reduced (DTT 20 mM for 60 min at 60°C) and

alkylated (iodoacetamide 55 mM for 30 min at 30°C) in the dark. The bands were digested for 16 h at 37°C with porcine trypsin (Sequencing Grade Modified Trypsin, 0.4 µg trypsin/sample; Promega). Finally, the resulting peptide mixture in each band was extracted from the gel matrix with 10% formic acid (FA) and ACN and dried. The peptide mixture was analyzed in a nano-ACQUITY LC (Waters) coupled to an LTQ-Orbitrap Velos (Thermo Fisher Scientific) MS. Tryptic peptides were resuspended in 1% FA solution, and an aliquot was injected for chromatographic separation. Peptides were trapped on a Symmetry C18TM trap column (5 µm × 180 µm × 20 mm; Waters), and they were separated using a C18 reverse-phase capillary column (75-µm Øi, 10 cm, nanoACQUITY, 1.7-µm BEH column; Waters). The gradient used for the elution of the peptides was 1%–40% B in 60 min followed by gradient from 40% to 60% in 10 min and a final step from 60% to 90% B in 5 min (A, 0.1% FA; B, 100% ACN; 0.1% FA), with a 250 nL/min flow rate. Eluted peptides were subjected to electrospray ionization in an emitter needle (PicoTip; New Objective) with an applied voltage of 2,000 V. Peptide masses (mass/charge ratio 350–1,700) were analyzed in data-dependent mode of a full-scan MS in the Orbitrap with a resolution of 60,000 full width at half maximum at mass/charge ratio 400. As many as the 10 most abundant peptides (minimum intensity of 500 counts) were selected from each MS scan and then fragmented using collision-induced dissociation in a linear ion trap (LTQ) using helium as the collision gas with 38% normalized collision energy. Generated raw data were collected with Xcalibur 2.2 software (Thermo Fisher Scientific), and for each sample, two LC-tandem MS runs were acquired. A database was created by merging all UniProt database entries for *Gallus gallus* (version 4/02/15). Proteome Discover (v.1.3.0.339) software (Thermo Fisher Scientific) was used to perform a search of this database with the SEQUEST search engine. Both a target and a decoy database were searched to obtain a false discovery rate (FDR) and estimate the number of incorrect peptide–spectrum matches that exceed a given threshold. To improve the sensitivity of the database search, Percolator (semisupervised learning machine) was used to discriminate correct from incorrect peptide–spectrum matches. Percolator assigns a q-value to each spectrum, which is defined as the minimal FDR at which the identification is deemed correct. These q-values are estimated from the score distributions of a decoy database search for each sample; the RAW file obtained in the MS analysis was used to search the database. The resulting MSF files of both samples have been merged with the search software, allowing the results to be exported as a single Excel file to better compare the results. The results were filtered so that only proteins identified with at least two high-confidence peptides (FDR ≤ 0.01) are included in the list.

In vivo luciferase reporter assay
Embryos were electroporated with the DNAs indicated together with a 5xTcf-BS luciferase reporter construct containing synthetic TCF binding sites (TOPFlash) as well as with a *Renilla reniformis* construct (Promega) for normalization. GFP+ NTs were dissected out at 48 hpe and homogenized in Passive Lysis Buffer. Firefly and *Renilla* luciferase activity was measured by the Dual Luciferase Reporter Assay System (Promega).

Immunoblotting
Purified fractions were mixed with 5× SDS Laemmli sample buffer (1× = 2% SDS, 65 mM Tris-HCl [pH 6.8], 10% glycerol, 100 mM DTT, and 0.5 mg/ml bromophenol blue), boiled for 5 min (or 20 min for cross-linked samples), resolved by SDS-PAGE (8% gels), and then transferred to nitrocellulose membranes. The membranes were blocked with Odyssey Blocking Buffer (OBB), incubated overnight at 4°C with the primary antibodies in OBB containing 0.2% Tween 20, washed three times with TBS with Tween 20 (150 mM NaCl, 0.1% Tween 20, and 20 mM Tris-HCl [pH 7.4]) and incubated with Alexa-labeled secondary antibodies in OBB containing 0.2% Tween 20 and 0.01% SDS. After three final washes in TBS with Tween 20, the membranes were allowed to dry, and the fluorescence was detected on an Odyssey Infrared Imaging System (LI-COR). The expression values were quantified with ImageJ software, and the molecular weights were calculated using Bio-Rad Precision Molecular Weight Markers. The values shown represent the mean ± SD of three independent experiments.

Immunohistochemistry
Embryos were fixed for 4 h (to HH20) or overnight (beyond HH20) at 4°C in 4% paraformaldehyde, and immunostaining was performed on vibratome sections (60 µm) while following standard procedures. After washing in 0.1% PBS + Triton X-100, the sections were incubated with the appropriate primary antibodies and developed with Alexa- or cyanine-conjugated secondary antibodies. After staining, the sections were mounted with Fluoromount (Sigma-Aldrich) and examined at 18°C on a Leica SP5 (20× NA 0.7, 40× NA 1.25) using Leica Application Suite software or a Zeiss LSM 780 (25× NA 0.57, 40× NA 1.3, 63× NA 0.18) multiphoton microscope using ZEN 2.1 software. Images were manipulated using ImageJ software.

HEK-293 cell fractionation
Confluent cultures of HEK-293 cells in 10-cm dishes were rinsed once with PBS (supplemented with 1 mM CaCl$_2$ and 1 mM MgCl$_2$), scraped off in 1 ml of ice-cold hypotonic buffer (1 mM sodium bicarbonate [pH 7.4], 10 µg/ml aprotinin, 10 µg/ml leupeptin, and 1 mM PMSF) and homogenized with a Glass/Teflon Potter-Elvehjem homogenizer. The lysates were transferred to 1.5-ml tubes and centrifuged at 1,000 ×g for 10 min at 4°C. The supernatant was decanted and the pellet homogenized again as described above. The two resultant supernatants were pooled and centrifuged at 25,000 ×g for 30 min at 4°C. The first and second pellets contained the internal membranes and the plasma membrane, respectively, and they were washed once with the same buffer and then resuspended in 1× Laemmli sample buffer.

Glycosidase and AP treatment
Aliquots of Strep-Tactin–purified proteins were used to study phosphorylation (with AP) and glycosylation (with EndoH or PNGase). Briefly, the AP reaction was performed at 37°C for 1 h

in a volume of 80 µl containing 40 µl Strep-Tactin–purified protein, 20 µg/ml aprotinin, 20 µg/ml leupeptin, 1 mM PMSF, 50 mM Tris-HCl (pH 9), 1 mM MgCl$_2$, and 2 µl calf intestine AP (30 U/µl, #2250A; Takara). For the EndoH reactions, 36 µl of purified protein was incubated at 100°C for 10 min with denaturing buffer (0.5% SDS and 40 mM DTT) in a final volume of 40 µl, and the volume was then raised to 80 µl by adding sodium citrate (pH 5.5) up to 50 mM. Each sample was then split into two and incubated in the presence or absence of 2 µl of EndoH (50 U/µl, #P0702S; New England Biolabs) for 1 h at 37°C. The PNGase-F reaction was performed as that with EndoH, but the reaction buffer contained 50 mM sodium phosphate (pH 7.5), 1% NP-40, and PNGase-F (50 U/µl, #P0704S; New England Biolabs).

Calculation of the Manders correlation coefficients

To analyze colocalization, images were acquired on either a Leica SP5 or a Zeiss LSM 780 confocal microscope; the area of interest was outlined manually in each dual-labeled confocal slice and then processed with the Coloc2 plugin of the Fiji version of ImageJ image processing software. To calculate the fraction of N-cadherin that colocalized with aPKC, β-catenin, GM130, or Golgin97, Manders coefficients were obtained for every region, with thresholds (Manders et al., 1993) and the associated Costes P values (Costes et al., 2004). For NTs, at least 10 different images were analyzed for each coefficient, whereas for cell cultures, 10 images were taken from each well, with two and three wells from different experiments analyzed for Golgin97 and GM130, respectively. All the coefficients were verified with the Costes statistical significance test.

Statistical analyses

In Fig. 3, B and F, Fig. 4 M, Fig. S1 N, and Fig. S3 E and F, each experimental condition was compared with every other experimental condition using a one-way ANOVA with Tukey's multiple comparisons test. For Fig. 2, G′–L′, each experimental condition was compared with its control condition using an unpaired t test. For Fig. 6, C and D, Fig. 8 I, Fig. S1 M, and Fig. S4 A, each experimental condition was compared with the respective control using a one-way ANOVA with a Dunnett's multiple comparisons test. All statistical analyses were performed using GraphPad Prism 6 software, and significance was assumed when *, $P < 0.05$; **, $P < 0.01$; and ***, $P < 0.001$.

Online supplemental material

Fig. S1 shows images of two staining combinations highlighting the most relevant tissue alterations presented in Fig. 2, A–F and the efficiency of Sh-CTNNB1 and the effect of the different tools used in Fig. 2, A–F on Wnt-dependent transcription. Fig. S2 confirms that N-cadherin translocation to the plasma membrane by β-catenin requires the β-catenin–binding domain of N-cadherin. Fig. S3 shows that furin activity on pro-N-cadherin requires the β-catenin–binding site of N-cadherin, that FXa-N-cadherin does not produce mature N-cadherin, and that β-cateninΔC has no transcriptional activity and confirms that FXa-N-cadherin binds and represses β-catenin transcriptional activity in a similar manner to N-cadherin. Fig. S4 shows the efficiency of the shRNAs targeting the Golgi proteins and the

images used to quantify the pro-N-cadherin and N-cadherin levels shown in Fig 6. Fig. S5 shows the effect of DBNL knockdown on the apico-basal polarity of NT, and it confirms that the two bands of Dbnl correspond to two phosphorylation states. Table S1 shows the MS analysis comparing the proteins binding to N-cadherin and/or to N-cadherinΔβcat. Table S2 shows the subcellular distribution of the proteins that bind to N-cadherin but not to N-cadherinΔβcat.

References

Baum, B., and M. Georgiou. 2011. Dynamics of adherens junctions in epithelial establishment, maintenance, and remodeling. *J. Cell Biol.* 192:907–917. https://doi.org/10.1083/jcb.201009141

Binder, J. X., S. Pletscher-Frankild, K. Tsafou, C. Stolte, S. I. O'Donoghue, R. Schneider, and L. J. Jensen. 2014. COMPARTMENTS: unification and visualization of protein subcellular localization evidence. *Database.* 2014(0):bau012-bau012.

Birchmeier, C., W. Birchmeier, and B. Brand-Saberi. 1996. Epithelial-mesenchymal transitions in cancer progression. *Acta Anat. (Basel).* 156:217–226. https://doi.org/10.1159/000147848

Carpenter, P.M., R.A. Al-Kuran, and C.P. Theuer. 2002. Paranuclear E-cadherin in gastric adenocarcinoma. *Am. J. Clin. Pathol.* 118:887–894. https://doi.org/10.1309/EKFB-0HJT-AB1D-5LJB

Chen, J., and M. Zhang. 2013. The Par3/Par6/aPKC complex and epithelial cell polarity. *Exp. Cell Res.* 319:1357–1364. https://doi.org/10.1016/j.yexcr.2013.03.021

Chen, Y.T., D.B. Stewart, and W.J. Nelson. 1999. Coupling assembly of the E-cadherin/beta-catenin complex to efficient endoplasmic reticulum exit and basal-lateral membrane targeting of E-cadherin in polarized

MDCK cells. *J. Cell Biol.* 144:687–699. https://doi.org/10.1083/jcb.144.4.687

Costes, S.V., D. Daelemans, E.H. Cho, Z. Dobbin, G. Pavlakis, and S. Lockett. 2004. Automatic and quantitative measurement of protein-protein colocalization in live cells. *Biophys. J.* 86:3993–4003. https://doi.org/10.1529/biophysj.103.038422

Das, R.M., and K.G. Storey. 2014. Apical abscission alters cell polarity and dismantles the primary cilium during neurogenesis. *Science.* 343: 200–204. https://doi.org/10.1126/science.1247521

Fucini, R.V., J.L. Chen, C. Sharma, M.M. Kessels, and M. Stamnes. 2002. Golgi vesicle proteins are linked to the assembly of an actin complex defined by mAbp1. *Mol. Biol. Cell.* 13:621–631. https://doi.org/10.1091/mbc.01-11-0547

Gottardi, C.J., E. Wong, and B.M. Gumbiner. 2001. E-cadherin suppresses cellular transformation by inhibiting beta-catenin signaling in an adhesion-independent manner. *J. Cell Biol.* 153:1049–1060. https://doi.org/10.1083/jcb.153.5.1049

Götz, M., and W.B. Huttner. 2005. The cell biology of neurogenesis. *Nat. Rev. Mol. Cell Biol.* 6:777–788. https://doi.org/10.1038/nrm1739

Grigoryan, T., P. Wend, A. Klaus, and W. Birchmeier. 2008. Deciphering the function of canonical Wnt signals in development and disease: conditional loss- and gain-of-function mutations of beta-catenin in mice. *Genes Dev.* 22:2308–2341. https://doi.org/10.1101/gad.1686208

Gujral, T.S., E.S. Karp, M. Chan, B.H. Chang, and G. MacBeath. 2013. Family-wide investigation of PDZ domain-mediated protein-protein interactions implicates β-catenin in maintaining the integrity of tight junctions. *Chem. Biol.* 20:816–827. https://doi.org/10.1016/j.chembiol.2013.04.021

Gumbiner, B.M. 2000. Regulation of cadherin adhesive activity. *J. Cell Biol.* 148:399–404. https://doi.org/10.1083/jcb.148.3.399

Hamburger, V., and H.L. Hamilton. 1992. A series of normal stages in the development of the chick embryo. 1951. *Dev. Dyn.* 195:231–272. https://doi.org/10.1002/aja.1001950404

Hanahan, D., and R.A. Weinberg. 2000. The hallmarks of cancer. *Cell.* 100: 57–70. https://doi.org/10.1016/S0092-8674(00)81683-9

Herrera, A., M. Saade, A. Menendez, E. Marti, and S. Pons. 2014. Sustained Wnt/β-catenin signalling causes neuroepithelial aberrations through the accumulation of aPKC at the apical pole. *Nat. Commun.* 5:4168. https://doi.org/10.1038/ncomms5168

Hill, M.A. 2021. Embryology Hamburger Hamilton Stages. https://embryology.med.unsw.edu.au/embryology/index.php/Hamburger_Hamilton_Stages (accessed April 26, 2021).

Hinck, L., I.S. Näthke, J. Papkoff, and W.J. Nelson. 1994. Dynamics of cadherin/catenin complex formation: novel protein interactions and pathways of complex assembly. *J. Cell Biol.* 125:1327–1340. https://doi.org/10.1083/jcb.125.6.1327

Huels, D.J., R.A. Ridgway, S. Radulescu, M. Leushacke, A.D. Campbell, S. Biswas, S. Leedham, S. Serra, R. Chetty, G. Moreaux, et al. 2015. E-cadherin can limit the transforming properties of activating β-catenin mutations. *EMBO J.* 34:2321–2333. https://doi.org/10.15252/embj.201591739

Inoue, S., K. Hayashi, K. Fujita, K. Tagawa, H. Okazawa, K.I. Kubo, and K. Nakajima. 2019. Drebrin-like (Dbnl) controls neuronal migration via regulating N-cadherin expression in the developing cerebral cortex. *J. Neurosci.* 39:678–691. https://doi.org/10.1523/JNEUROSCI.1634-18.2018

Jeanes, A., C.J. Gottardi, and A.S. Yap. 2008. Cadherins and cancer: how does cadherin dysfunction promote tumor progression? *Oncogene.* 27: 6920–6929. https://doi.org/10.1038/onc.2008.343

Kim, C.H., T. Oda, M. Itoh, D. Jiang, K.B. Artinger, S.C. Chandrasekharappa, W. Driever, and A.B. Chitnis. 2000. Repressor activity of Headless/Tcf3 is essential for vertebrate head formation. *Nature.* 407:913–916. https://doi.org/10.1038/35038097

Klockenbusch, C., and J. Kast. 2010. Optimization of formaldehyde cross-linking for protein interaction analysis of non-tagged integrin beta1. *J. Biomed. Biotechnol.* 2010:927585. https://doi.org/10.1155/2010/927585

Kojima, S., and G.G. Borisy. 2014. An image-based, dual fluorescence reporter assay to evaluate the efficacy of shRNA for gene silencing at the single-cell level. *F1000 Res.* 3:60. https://doi.org/10.12688/f1000research.3-60.v2

Kubben, N., J.W. Voncken, J. Demmers, C. Calis, G. van Almen, Y. Pinto, and T. Misteli. 2010. Identification of differential protein interactors of lamin A and progerin. *Nucleus.* 1:513–525. https://doi.org/10.4161/nucl.1.6.13512

Larue, L., C. Antos, S. Butz, O. Huber, V. Delmas, M. Dominis, and R. Kemler. 1996. A role for cadherins in tissue formation. *Development.* 122: 3185–3194.

Le Bras, S., I. Foucault, A. Foussat, C. Brignone, O. Acuto, and M. Deckert. 2004. Recruitment of the actin-binding protein HIP-55 to the immunological synapse regulates T cell receptor signaling and endocytosis. *J. Biol. Chem.* 279:15550–15560. https://doi.org/10.1074/jbc.M312659200

Manders, E.M.M., F.J. Verbeek, and J.A. Aten. 1993. Measurement of colocalization of objects in dual-colour confocal images. *J. Microsc.* 169: 375–382. https://doi.org/10.1111/j.1365-2818.1993.tb03313.x

Manoranjan, B., C. Venugopal, D. Bakhshinyan, A.A. Adile, L. Richards, M.M. Kameda-Smith, O. Whitley, A. Dvorkin-Gheva, M. Subapanditha, N. Savage, et al. 2020. Wnt activation as a therapeutic strategy in medulloblastoma. *Nat. Commun.* 11:4323. https://doi.org/10.1038/s41467-020-17953-4

Maret, D., E. Gruzglin, M.S. Sadr, V. Siu, W. Shan, A.W. Koch, N.G. Seidah, R.F. Del Maestro, and D.R. Colman. 2010. Surface expression of precursor N-cadherin promotes tumor cell invasion. *Neoplasia.* 12: 1066–1080. https://doi.org/10.1593/neo.10954

Maret, D., M.S. Sadr, E.S. Sadr, D.R. Colman, R.F. Del Maestro, and N.G. Seidah. 2012. Opposite roles of furin and PC5A in N-cadherin processing. *Neoplasia.* 14:880–892. https://doi.org/10.1593/neo.121250

Marthiens, V., and C. ffrench-Constant. 2009. Adherens junction domains are split by asymmetric division of embryonic neural stem cells. *EMBO Rep.* 10:515–520. https://doi.org/10.1038/embor.2009.36

McEwen, A.E., M.T. Maher, R. Mo, and C.J. Gottardi. 2014. E-cadherin phosphorylation occurs during its biosynthesis to promote its cell surface stability and adhesion. *Mol. Biol. Cell.* 25:2365–2374. https://doi.org/10.1091/mbc.e14-01-0690

Megason, S.G., and A.P. McMahon. 2002. A mitogen gradient of dorsal midline Wnts organizes growth in the CNS. *Development.* 129: 2087–2098.

Miyashita, Y., and M. Ozawa. 2007. A dileucine motif in its cytoplasmic domain directs beta-catenin-uncoupled E-cadherin to the lysosome. *J. Cell Sci.* 120:4395–4406. https://doi.org/10.1242/jcs.03489

Nakamura, T., T. Hayashi, Y. Nasu-Nishimura, F. Sakaue, Y. Morishita, T. Okabe, S. Ohwada, K. Matsuura, and T. Akiyama. 2008. PX-RICS mediates ER-to-Golgi transport of the N-cadherin/beta-catenin complex. *Genes Dev.* 22:1244–1256. https://doi.org/10.1101/gad.1632308

Nakamura, T., T. Hayashi, Y. Mimori-Kiyosue, F. Sakaue, K. Matsuura, S. Iemura, T. Natsume, and T. Akiyama. 2010. The PX-RICS-14-3-3zeta/theta complex couples N-cadherin-beta-catenin with dynein-dynactin to mediate its export from the endoplasmic reticulum. *J. Biol. Chem.* 285: 16145–16154. https://doi.org/10.1074/jbc.M109.081315

Nakayama, K. 1997. Furin: a mammalian subtilisin/Kex2p-like endoprotease involved in processing of a wide variety of precursor proteins. *Biochem. J.* 327:625–635. https://doi.org/10.1042/bj3270625

Nelson, W.J., and R. Nusse. 2004. Convergence of Wnt, beta-catenin, and cadherin pathways. *Science.* 303:1483–1487. https://doi.org/10.1126/science.1094291

Nelson, E.R., S. Li, M. Kennedy, S. Payne, K. Kilibarda, J. Groth, M. Bowie, E. Parilla-Castellar, G. de Ridder, P.K. Marcom, et al. 2016. Chemotherapy enriches for an invasive triple-negative breast tumor cell subpopulation expressing a precursor form of N-cadherin on the cell surface. *Oncotarget.* 7:84030–84042. https://doi.org/10.18632/oncotarget.12767

Niwa, H., K. Yamamura, and J. Miyazaki. 1991. Efficient selection for high-expression transfectants with a novel eukaryotic vector. *Gene.* 108: 193–199. https://doi.org/10.1016/0378-1119(91)90434-D

Pöschl, J., M. Bartels, J. Ohli, E. Bianchi, K. Kuteykin-Teplyakov, D. Grammel, J. Ahlfeld, and U. Schüller. 2014. Wnt/β-catenin signaling inhibits the Shh pathway and impairs tumor growth in Shh-dependent medulloblastoma. *Acta Neuropathol.* 127:605–607. https://doi.org/10.1007/s00401-014-1258-2

Rabadán, M.A., A. Herrera, L. Fanlo, S. Usieto, C. Carmona-Fontaine, E.H. Barriga, R. Mayor, S. Pons, and E. Martí. 2016. Delamination of neural crest cells requires transient and reversible Wnt inhibition mediated by Dact1/2. *Development.* 143:2194–2205. https://doi.org/10.1242/dev.134981

Rogers, C.D., L.K. Sorrells, and M.E. Bronner. 2018. A catenin-dependent balance between N-cadherin and E-cadherin controls neuroectodermal cell fate choices. *Mech. Dev.* 152:44–56. https://doi.org/10.1016/j.mod.2018.07.003

Rousso, D.L., C.A. Pearson, Z.B. Gaber, A. Miquelajauregui, S. Li, C. Portera-Cailliau, E.E. Morrisey, and B.G. Novitch. 2012. Foxp-mediated suppression of N-cadherin regulates neuroepithelial character and progenitor maintenance in the CNS. *Neuron.* 74:314–330. https://doi.org/10.1016/j.neuron.2012.02.024

Saade, M., I. Gutiérrez-Vallejo, G. Le Dréau, M.A. Rabadán, D.G. Miguez, J. Buceta, and E. Martí. 2013. Sonic hedgehog signaling switches the mode

of division in the developing nervous system. *Cell Rep.* 4:492–503. https://doi.org/10.1016/j.celrep.2013.06.038

Staal, F.J., B.M. Burgering, M. van de Wetering, and H.C. Clevers. 1999. Tcf-1-mediated transcription in T lymphocytes: differential role for glycogen synthase kinase-3 in fibroblasts and T cells. *Int. Immunol.* 11:317–323. https://doi.org/10.1093/intimm/11.3.317

Stockinger, A., A. Eger, J. Wolf, H. Beug, and R. Foisner. 2001. E-cadherin regulates cell growth by modulating proliferation-dependent beta-catenin transcriptional activity. *J. Cell Biol.* 154:1185–1196. https://doi.org/10.1083/jcb.200104036

Taverna, E., F. Mora-Bermúdez, P.J. Strzyz, M. Florio, J. Icha, C. Haffner, C. Norden, M. Wilsch-Bräuninger, and W.B. Huttner. 2016. Non-canonical features of the Golgi apparatus in bipolar epithelial neural stem cells. *Sci. Rep.* 6:21206. https://doi.org/10.1038/srep21206

Valenta, T., M. Gay, S. Steiner, K. Draganova, M. Zemke, R. Hoffmans, P. Cinelli, M. Aguet, L. Sommer, and K. Basler. 2011. Probing transcription-specific outputs of β-catenin in vivo. *Genes Dev.* 25:2631–2643. https://doi.org/10.1101/gad.181289.111

Wahl, J.K. III, Y.J. Kim, J.M. Cullen, K.R. Johnson, and M.J. Wheelock. 2003. N-cadherin-catenin complexes form prior to cleavage of the proregion and transport to the plasma membrane. *J. Biol. Chem.* 278:17269–17276. https://doi.org/10.1074/jbc.M211452200

Zhu, L., P. Gibson, D.S. Currle, Y. Tong, R.J. Richardson, I.T. Bayazitov, H. Poppleton, S. Zakharenko, D.W. Ellison, and R.J. Gilbertson. 2009. Prominin 1 marks intestinal stem cells that are susceptible to neoplastic transformation. *Nature.* 457:603–607. https://doi.org/10.1038/nature07589
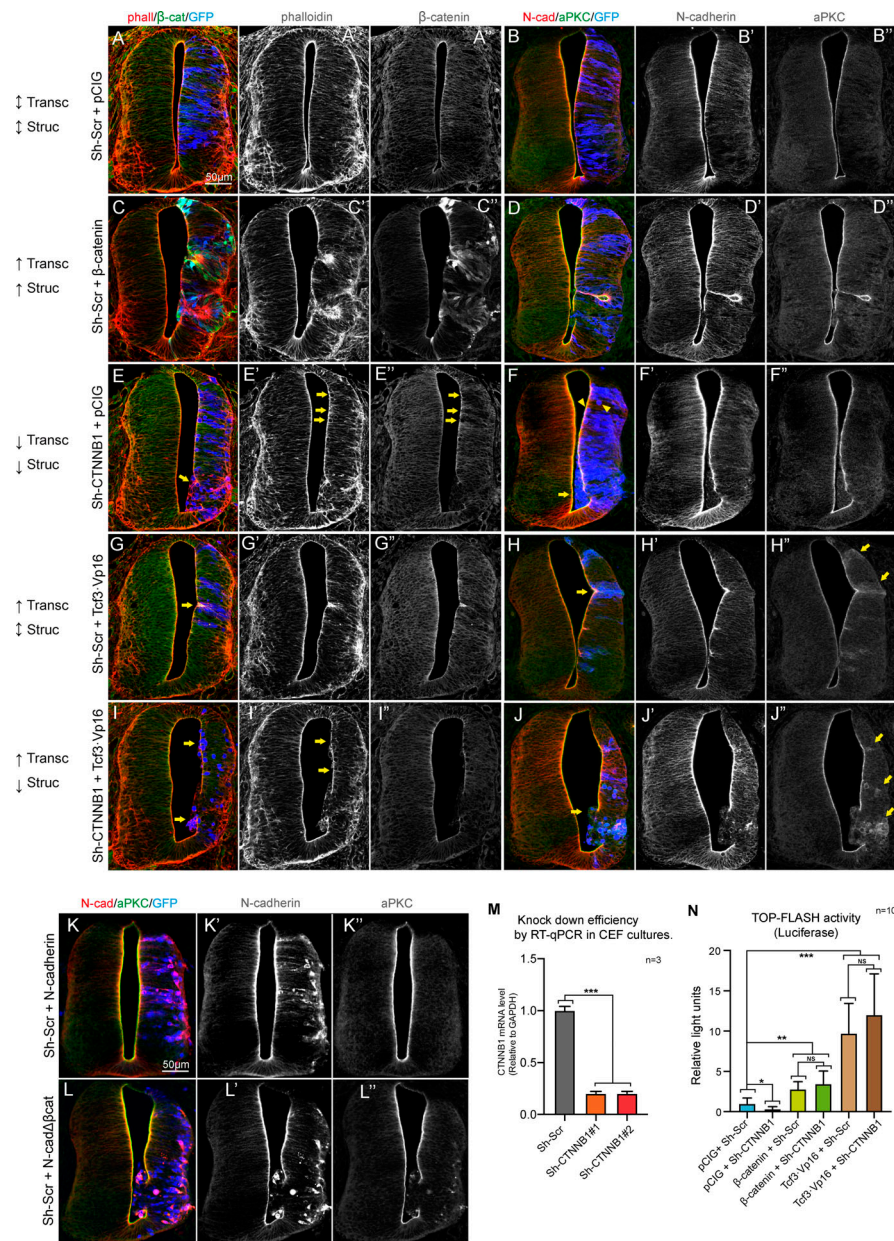
Supplemental material

Figure S1. **β-catenin induces apical localization of aPKC through its binding to N-cadherin. (A–J)** HH23 chicken NTs 48 hpe with different molecular tools intended to independently manipulate the transcriptional (Transc) and structural (Struc) activities of β-catenin. The expected effect caused by each tool on the transcriptional and structural activities is indicated to the left of each row as follows: ↑, increased activity; ↓, decreased activity; ↑↓, no change. In addition, pCIG stands for the empty vector; β-catenin is a stable form of β-catenin (β-catenin^{S33Y}), Sh-Scr and Sh-CTNNB1 are scrambled and anti-β-catenin inhibitory shRNAs, respectively. Tcf3·Vp16 is a constitutive activator of TCF-dependent transcription, and N-cadherinΔβcat is the N-cadherin mutant lacking the β-catenin–binding domain. The figure shows representative images of the transfected NTs used for the quantification in Fig. 2, and the channels are shown separately in grayscale for clarity. In panels A, C, E, G, and I, the slices were stained for F-actin (phalloidin, red), β-catenin (green), and GFP (blue, indicating transfection). Panels B, D, F, H, and J were stained for N-cadherin (red), aPKC (green), and GFP (blue, indicating transfection). The arrows in panels E, E', and E'' indicate Sh-CTNNB1–transfected cells with a round morphology, some of them protruding into the ventricle. Knockdown of β-catenin by Sh-CTNNB1 is evident in panel E''. In panel F, the arrowheads and arrow point to round and protruding cells, respectively. In panels G and H, the arrows pinpoint small invaginations caused by Tcf3·Vp16, while the arrows in panel H'' indicate the accumulation of cytoplasmic aPKC in the transfected areas. Arrows in panel I and I' point to cells protruding into the ventricle, and the arrows in panel J'' denote the accumulation of cytoplasmic aPKC in cells expressing a combination of Tcf3·Vp16 and Sh-CTNNB1. Note that in this case, the knockdown of β-catenin caused a loss of apico-basal polarity rather than the typical small invaginations normally induced by Tcf3·Vp16. **(K and L)** HH12 chicken NTs transfected with wild-type N-cadherin (K) or N-cadherinΔβcat (L) stained with antibodies against N-cadherin (red) and aPKC (green) 48 h later. GFP is shown in blue, indicating transfection. **(M)** Knockdown efficiency of two different inhibitory shRNAs targeting CTNNB1 studied by quantitative RT-PCR (RT-qPCR) in chicken embryonic fibroblasts (CEFs). Each experimental condition was compared with its control condition using an unpaired t test (n = 3). **(N)** Wnt pathway activity (TOPFlash) studied by a luciferase reporter assay in HH18 chicken NTs 24 hpe with control, Sh-CTNNB1, β-catenin, Sh-CTNNB1 plus β-catenin, Tcf3·Vp16, or Tcf3·Vp16 plus Sh-CTNNB1. Bar graphs show the mean ± SD. Each experimental condition was compared with every other experimental condition using a one-way ANOVA with Tukey's multiple comparisons test (n = 10). *, P < 0.05; **, P < 0.01; ***, P < 0.001. cad, cadherin.
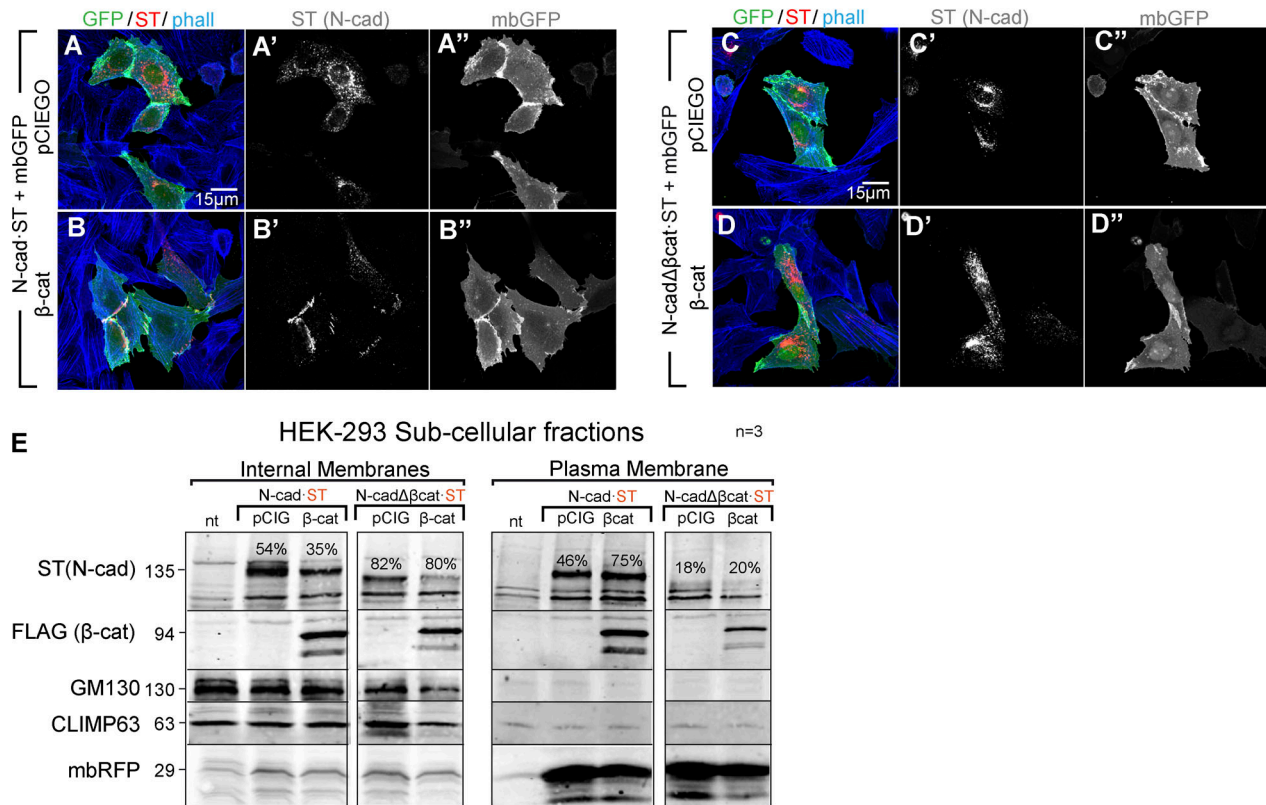
Figure S2. **β-catenin promotes the delivery of N-cadherin to intercellular junctions. (A and B)** HEK-293 cells 24 hpe with N-cadherin with (B–B'') or without (A–A'') β-catenin. The cells were stained with antibodies against N-cadherin (red) and phalloidin (phall; F-actin, blue), while mbGFP (green) was used to define the plasma membrane of the transfected cells. **(C and D)** A similar experiment as in A but with N-cadherinΔβcat. **(E)** Fractions enriched in internal membranes or plasma membranes were generated from HEK-293 cells transfected with N-cadherin or N-cadherinΔβcat plus β-catenin or the control vector. The proportion of protein detected in the internal and the plasma membrane fractions was calculated for N-cadherin and N-cadherinΔβcat in each condition and is indicated in each lane. CLIMP63 and GM130 were used as ER and Golgi markers, respectively, and transfected mbRFP was used as a plasma membrane marker (n = 3). cad, cadherin.
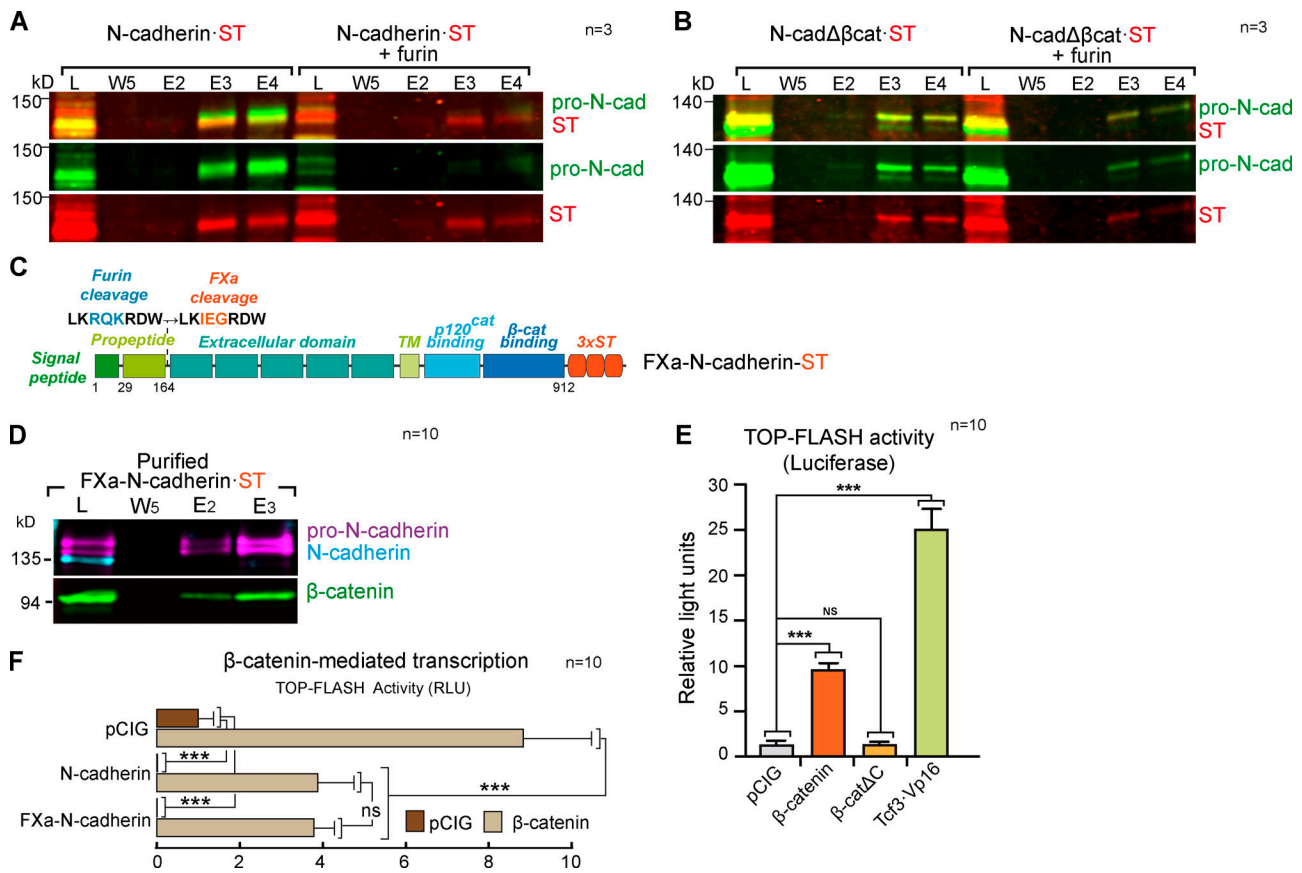
Figure S3. **The β-catenin–binding domain of N-cadherin is required for furin-mediated propeptide cleavage. (A)** Western blot showing Strep-Tactin–purified fractions of HEK-293 cultures transfected with a control vector or a vector expressing furin and N-cadherin·ST. The blot was probed with antibodies against pro-N-cadherin (green) and ST (red); $n = 3$. **(B)** As in A, but with N-cadherinΔβcat. **(C)** Scheme of the FXa-N-cadherin·ST construct in which the furin cleavage site on N-cadherin has been substituted with an FXa site similar in size but not cleavable in the cell ($n = 3$). **(D)** Western blot showing Strep-Tactin–purified fractions of HH18 chicken NTs transfected with FXa-N-cadherin·ST and probed with antibodies against pro-N-cadherin (purple), N-cadherin (cyan), and β-catenin (green). Note that FXa-N-cadherin·ST does not generate mature N-cadherin ($n = 10$). **(E)** Wnt pathway activity (TOPFlash) studied with a luciferase reporter assay in HH18 chicken NTs 24 hpe with control, β-catenin, β-cateninΔC, β-catenin, or Tcf3·Vp16. Bar graphs show the mean ± SD. Each experimental condition was compared with every other experimental condition using a one-way ANOVA with Tukey's multiple comparisons test ($n = 10$). **(F)** The bar graph represents the mean ± SD (three independent experiments) of luciferase reporter assays using TOPFlash vector 48 hpe with pCIG, N-cadherin, or FXa-N-cadherin cotransfected with β-catenin or not. Each experimental condition was compared with every other experimental condition using a one-way ANOVA with Tukey's multiple comparisons test ($n = 10$). ***, P < 0.001. cad, cadherin; E, elution; L, lysate; RLU, relative light unit; TM, transmembrane domain; W, wash.
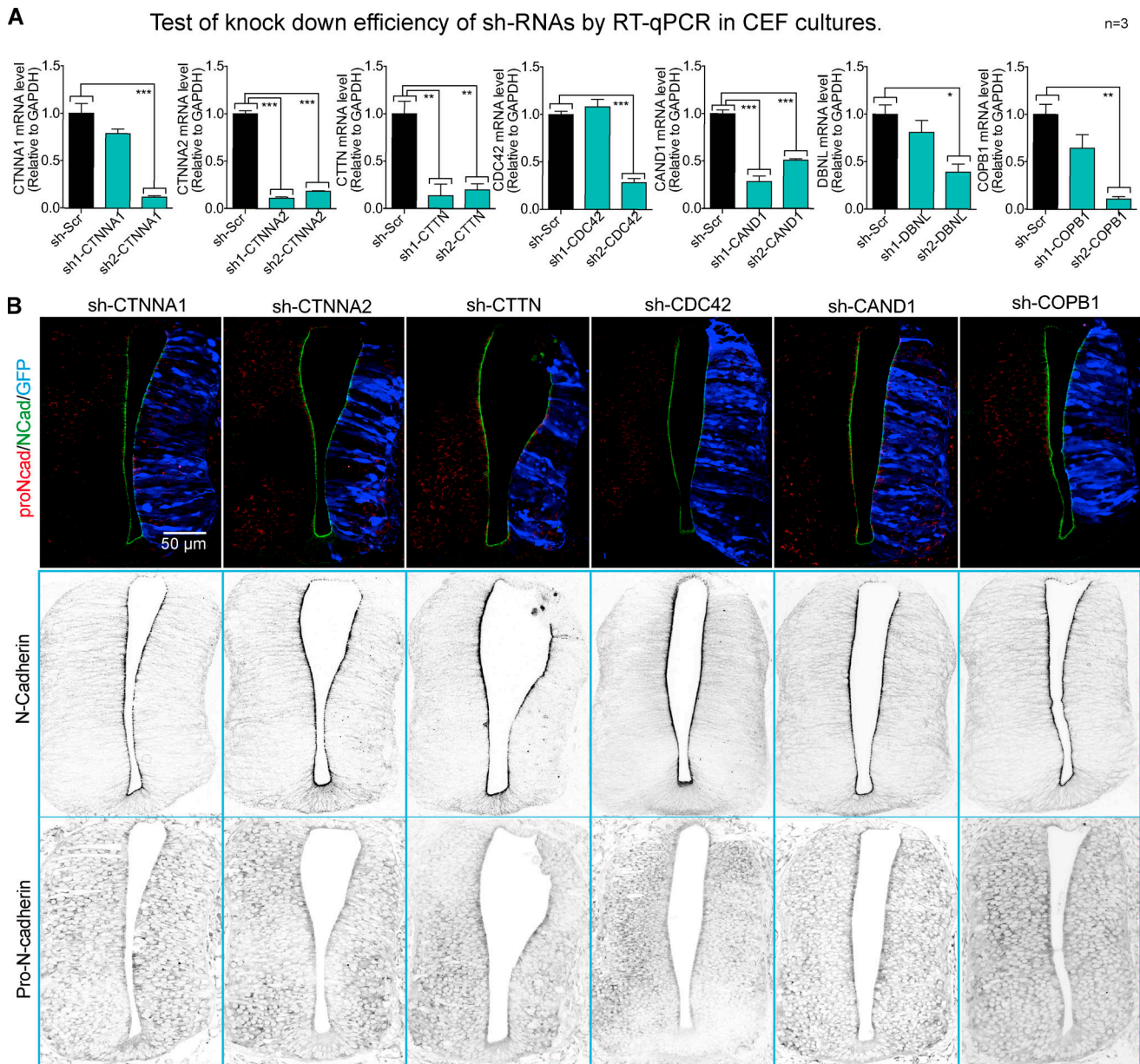
A   Test of knock down efficiency of sh-RNAs by RT-qPCR in CEF cultures.   n=3

B

Figure S4. **New β-catenin–dependent interactions of N-cadherin implicated in its maturation. (A)** shRNAs targeting each of the seven proteins predicted to be in the Golgi apparatus were cloned into the pSHIN vector. Two different shRNAs were designed for each gene, and their knockdown efficiency was tested by quantitative RT-PCR (RT-qPCR) in chicken embryonic fibroblasts (CEFs). Each experimental condition was compared with the respective control using a one-way ANOVA with Dunnett's multiple comparisons test (*n* = 3). **(B)** The most efficient shRNA of each pair was electroporated in HH12 chicken NTs, and slices were stained with pro-N-cadherin (red) and N-cadherin (green) at 48 hpe. GFP denoting transfection is shown in blue. Channels are shown separately in grayscale for clarity. The bar graphs show the mean ± SD. *, P < 0.05; **, P < 0.01; ***, P < 0.001. cad, cadherin; Scr, scramble.

C

Chicken Dbnl potential phosphorylation motifs

MALNLSKNGRALQEAYGRVVAAGSPTDWALFTYEGNSNDLRVAGSGEGGL
EEMVEELNSGKVMYAFCRVKDPNSGLPKYVLVNWTGEGVNDVRKGACANH
VSTIASFLKGAHVTINARAEEDVEPELIMQKVAKASGANYSFHKESSRFQ
DAGPQGPVGSVYQKTNAMSEIKRVNKDHFWAKAEKDEENRRLEEKRRAEE
ERQRLERERRERELREAAGREQRFQARSSQIEAQKRLQQEAERREQQQWK
EQQQAEEHEAGQRRSVRRSESVEKAQEAASLIAQRPGNPRDIFVQRERAA
PGDTAAAAQPGKLRSPFLQREQDEVPTPTPTTPDPSRVSAAGHNVSPMGT
HMDGENVYEDAADSTAIYEEPPQDHDDGAQYQYPGGYQQEPELAGKGLCA
RALYDYQAADDTEISFDPENIITNIEMIDEGWWRGYGPDGHFGMFPANYV
ELLE

Tyrosine kinase / phosphatase motifs (15)
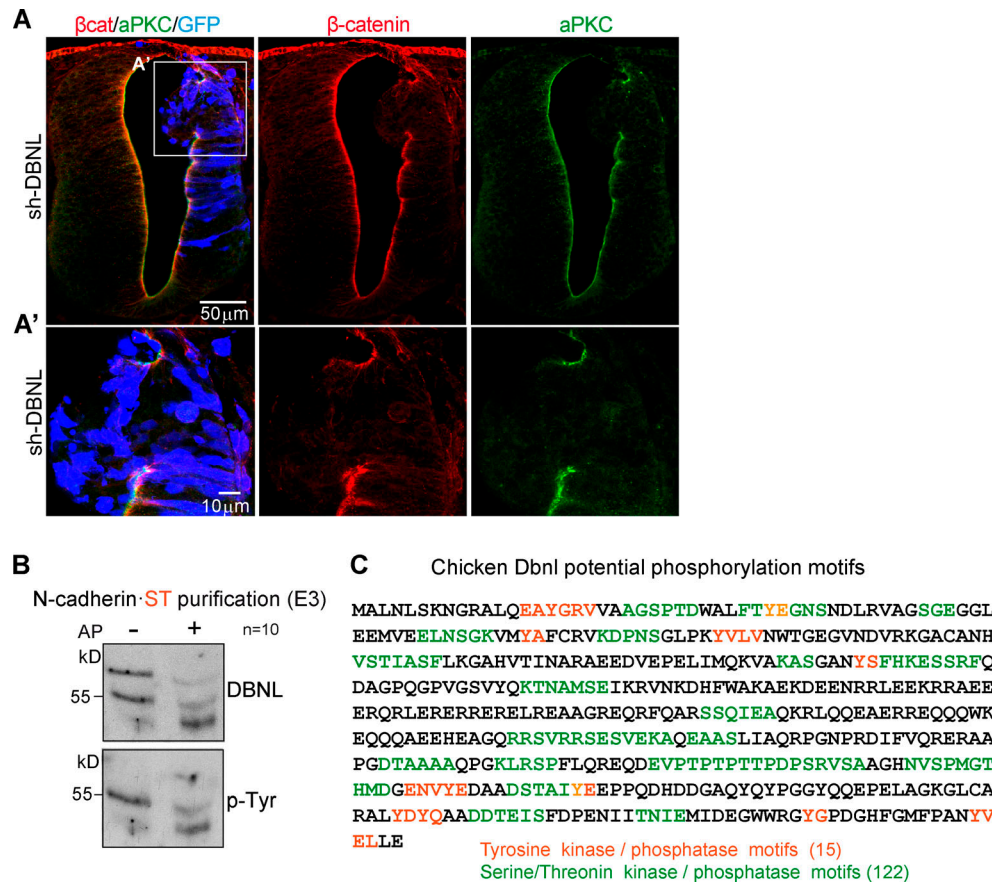Serine/Threonin kinase / phosphatase motifs (122)

Figure S5. **DBNL knockdown disrupts the apico-basal polarity of chicken NT. (A and A')** HH23 chicken NTs were stained with β-catenin (red), aPKC (green), and GFP (blue, indicates transfection) 48 hpe with sh-DBNL. **(B)** Western blot of N-cadherin·ST–purified fractions untreated or treated with AP. The membrane was sequentially incubated with antibodies against Dbnl and phospho-Tyr. Note that the two Dbnl bands turned into a single band of lower molecular weight upon AP treatment, indicating that the difference between the two Dbnl bands was due to their distinct phosphorylation status. Note also that only the lower band was phosphorylated at Tyr (n = 10). **(C)** Scheme of the reported phosphorylation sites in chicken Dbnl as predicted with the PhosphoMotif finder tool (http://hprd.org/PhosphoMotif_finder); note that each individual Tyr, Ser or Thr may be part of different phosphorylation motifs.

Table S1 and Table S2 are provided online as separate Excel files. Table S1 provides mass spectroscopy analysis comparing the proteins binding to N-cadherin and/or to N-cadherinΔβcat. Table S2 displays the subcellular distribution of the proteins that bind to N-cadherin but not to N-cadherinΔβcat.